The set-up of a RICO shallow cumulus case for LES

An internship at the:

Royal Netherlands Meteorological Institute (KNMI)

Louise Nuijens

July 23, 2006

The set-up of a RICO shallow cumulus case for LES

An internship at the:

Royal Netherlands Meteorological Institute (KNMI)

Supervisors:

A.P. Siebesma and M.C. van Zanten

Atmospheric Research Division, KNMI
Wilhelminalaan 10, 3732 GK, De Bilt, The Netherlands.

Louise Nuijens
MSc student Wageningen UR[1]

July 23, 2006

[1] Wageningen University and Research Center, Meteorology and Air Quality Section,
Building no.403, Duivendaal 2, 6701 AP Wageningen, The Netherlands.
E-mail: louise.nuyens@wur.nl

Preface

This report gives an overview of the work performed during my research internship, an obligatory part of the MSc program Meteorology and Air Quality (MAQ-70424), consisting of 24 ECTS (European credits). This internship was carried out at the Atmospheric Research Division of the Royal Netherlands Meteorological Institute (KNMI), under the supervision of A.P. Siebesma and M.C. van Zanten, during a period of 4 months.

The overall subject of my internship was to help with the set-up and preparation of a new intercomparison case for LES, an initiative of the GCSS (Global Water and Energy Experiment Cloud System Studies) Working Group on Boundary Layer Clouds (GCSS-WGBLC), currently led by A.P Siebesma. This new intercomparison is based on the Rain In Cumulus over the Ocean (RICO) Experiment that has been conducted in the period from November 2004 - January 2005. The LES case is therefore meant to study the dynamics of precipitating cumulus clouds. The final case set-up has been released in May 2006 on the KNMI website[1].

At the start of this internship I was unfamiliar with LES and during the four months of work I was mostly involved with the set-up of the RICO case, thereby using LES as a tool to study cumulus dynamics. My interpretation and description of the LES model in this report may therefore be rudimentory and in addition focused on the specific LES version for cumulus.

Because Pier and Margreet are leading the LES intercomparison case based on RICO, they were both closely involved with my work. An enthusiastic supervisor is basically the best thing that can happen to a student, and I was very lucky because I got two of them! I very much enjoyed this work, and I am interested to see the outcome and results of the intercomparison.

Beside my supervisors, I would like to acknowledge and thank the following persons at KNMI for their work and help with the RICO LES case. Erik van Meijgaard performed several RACMO runs and provided me with the output data of these runs, which were very useful to estimate large-scale forcings. Radiation profiles were provided by Alexander Los, who performed several runs with the MODTRAN radiation scheme, and by Gerd-Jan van Zadelhoff, who performed runs with the ECMWF radiation scheme. Lastly, I want to thank everyone at KNMI for creating such a pleasant and convenient working environment.

Louise Nuijens
July 23, 2006

[1] www.knmi.nl/samenw/rico

Contents

Chapter 1

Introduction

At present, Large Eddy Simulation (LES) is a widely used tool to study a variety of boundary layer and mesoscale phenomena, ranging from stable boundary layers to cloud-topped boundary layers. As its name reveals, LES is a three-dimensional modeling technique in which the largest turbulent eddies in an atmospheric flow are explicitly calculated, whereas the smaller turbulent motions are parameterized. LES is based on the well-known set of conservation equations for momentum, mass, heat and moisture, that are solved numerically on a three dimensional grid. Typical domain sizes of LES are of a few kilometers, with a resolution of a few tens of meters. Although simulations with LES can only be performed on limited domain and time scales, it has proven to be very succesful in simulating turbulent flow and is thus used to study processes and patterns in the atmospheric boundary layer. Moreover, LES is very useful to test new parameterization schemes.

The overall and most important goal of the GCSS (Global Water and Energy Experiment Cloud System Studies) Working Group on Boundary Layer Clouds (GCSS-WGBLC) is to improve physical parameterizations of boundary layer processes in Global Climate Models (GCM's), with a special attention to boundary layer clouds. Both stratocumulus and shallow cumulus have been the focus of the group in previous years. The group has used LES for these intercomparison studies, in combination with observations from various experiments. For instance, the study aimed at the dynamics of trade wind cumuli was based on the Atlantic Trade Wind Experiment (ATEX) (Stevens et al., 2001), and another study focused more on cumulus characteristics in general and used observations from the Barbados Oceanographic and Meteorological Experiment (BOMEX) (Siebesma et al., 2003). Many institutes and universities contribute to such intercomparison studies, in which they all use the exact same initialization set (initial and boundary conditions) but with slightly modified parameterizations or discretization schemes. By doing so, one can get a feeling of the sensitivity of LES to different schemes and discuss whether variability is a result of the used algorithms or whether it is a realistic representation of a turbulent atmospheric boundary layer.

Although the focus of previous LES studies on shallow cumulus has been on different processes and questions, they had one major thing in common: all the LES versions used for these intercomparisons assumed that the influence of any precipitation produced by shallow cumulus was negligible. Microphysics of shallow cumulus were therefore not included or parameterized in LES. However, recent analyses have shown that shallow precipitation occurs frequently (Petty, 1999; Short and Nakamura, 2000) and thus questions

have arised asking how and to what extent this may impact boundary layer dynamics (Jensen et al., 2000; Lau and Wu, 2003; von Salzen et al., 2005). During the past few years an increasing group of researchers has been interested in the dynamics and microphysics of shallow (trade wind) cumuli and their role in the global circulation and climate on earth. Recently a unique field experiment has been conducted: the Rain In Cumulus over the Ocean Experiment, focusing in specific on precipitation processes associated with shallow cumulus in the trade wind regions. During RICO, precipitation has been observed frequently and with significant amounts.

The unique dataset of RICO offers great opportunities to study the dynamics of shallow cumuli and precipitation, from a modeling perspective as well as an observational perspective. A start has yet been made with the implementation and testing of microphysical processes in shallow cumulus in the current LES versions. A.P. Siebesma and M.C. van Zanten, both affilliated at KNMI, have taken the initiative to set up an LES intercomparison case and base this case on observations performed during RICO. In the first place the aim of the new intercomparison case is to test these microphysical schemes and compare them. Second, an attempt will be made to simulate the cumulus dynamics and precipitation as observed during RICO.

The preparation of the case involves the selection of a specific day or period during, on which typical trade wind cumuli were present and a modest amount of rain was observed. Ideally a variety of measurements has been performed on such a day or period, giving the opportunity to prepare a basic inititalization set for LES that is based on these observations and thus conforms to the real, observed, situation as much as possible. Initially, one particular day (January 11, 2005) was favored for the LES case, but as observations on that day were analyzed and simulations were performed, the focus shifted to simulate the mean state of the atmosphere during a suppressed period of three weeks during RICO. The selection of interesting periods, the analysis of observations and using these in LES, in other words: preparing the initialization set for the LES precipitating cumulus case, was the main subject of this research internship. The initialization set for LES basically consists of the initial and boundary conditions that are needed to start any simulation. The initial conditions include for example the vertical profiles of temperature, moisture and winds. The boundary conditions include the surface conditions, the surface fluxes, and the large-scale forcings *i.e.*, large-scale advection, subsidence and radiation. As LES can be rather sensitive to the prescribed conditions, it is desired to test these conditions and adjust them if necessary to ensure that the cloud acitivity in LES is in equilibrium with the prescribed forcings leading to a steady state situation. A budget analysis can be performed to get a feeling of the balance between the prescribed forcings and the cloud field generated in LES. The tendencies for temperature and humidity, which are caused by all forcings acting on the model, can be estimated and used to construct heat and moisture budgets.

In *Chapter 2* we summarize the conservation equations on which LES is based and we describe what is needed to prepare a basic inititalization set for LES. A short overview of the RICO field study and our motivations for chosing a particular period during RICO are discussed. Observations gathered during RICO and a Regional Atmospheric Climate Model (RACMO) are used to deduce all forcings and initial conditions for the case. The results and findings of this observational and model analysis are discussed in *Chapter 3*. The analysis of the heat and moisture budgets and the results of LES runs performed

with the final initialization set are given in *Chapter 4*. In the last chapter, *Chapter 5* our motivations and the outcome of the case set-up are shortly summarized.

Chapter 2

The set-up of a LES case based on RICO

Setting up the RICO LES case involved specifying and continuously testing the initial and boundary conditions of the model. The specified conditions ideally led to a simulation in which the large-scale forcings are in reasonable balance and whose results are in agreement with the observations. A reliable set of specified conditions would then be a good basis for further simulations and studies.

In this chapter the general characteristics of the LES model are described. An overview of the exact initial and boundary conditions that are part of the desired initialization set for LES is given. Because this LES case focuses on precipitating shallow cumulus, it is based on observations obtained during the Rain In Cumulus over the Ocean field study. A short overview of the RICO field study is given here, and specific periods or days during RICO are considered for the case.

2.1 General characteristics of Large Eddy Simulation

LES is high-resolution three-dimensional model in which the largest turbulent eddies are explicitly solved. Turbulent motions or eddies on scales smaller than the gridsize of the model, so-called subgrid eddies, are parameterized. To do so, the well-known behaviour of turbulence on scales in the inertial subrange is used. Many detailed descriptions of the parameterizations in LES are available among which Cuijpers and Duynkerke (1993); Van Zanten (2000); Siebesma et al. (2003).

The typical gridsize of the model is a hundred meters in the horizontal and about 40 m in the vertical, and the total LES domain usually consists of a few kilometers in all directions. The mean state of the atmosphere in LES is predicted by the set of prognostic equations for the following variables: the x, y and z components of the horizontal wind, u and v and w, the liquid water potential temperature θ_l and the total water specific humidity q_t.

2.1.1 The budget equations for heat, moisture and momentum

The prognostic equations for momentum, heat and moisture are here presented as budget equations, in which all terms are averaged over the LES domain. We are mostly interested

in these mean terms, as they will determine the dynamics of the horizontal average fields in LES. The budget equations for the horizontal wind field, the liquid water potential temperature and total specific humidity are written as follows, with the overbars indicating an average over the LES domain:

$$\frac{\partial \overline{u}}{\partial t} + \overline{u}\frac{\partial \overline{u}}{\partial x} + \overline{v}\frac{\partial \overline{u}}{\partial y} + \overline{w}\frac{\partial \overline{u}}{\partial z} = f_c\left(\overline{v} - \overline{v}_g\right) - \frac{\partial\left(\overline{w'u'}\right)}{\partial z} \tag{2.1}$$

$$\frac{\partial \overline{v}}{\partial t} + \overline{u}\frac{\partial \overline{v}}{\partial x} + \overline{v}\frac{\partial \overline{v}}{\partial y} + \overline{w}\frac{\partial \overline{v}}{\partial z} = -f_c\left(\overline{u} - \overline{u}_g\right) - \frac{\partial\left(\overline{w'v'}\right)}{\partial z} \tag{2.2}$$

$$\frac{\partial \overline{\theta_l}}{\partial t} + \overline{u}\frac{\partial \overline{\theta)l}}{\partial x} + \overline{v}\frac{\partial \overline{\theta_l}}{\partial y} + \overline{w}\frac{\partial \overline{\theta_l}}{\partial z} = -\frac{1}{\overline{\rho}C_p}\frac{\partial \overline{F_z}}{\partial z} - \frac{\partial\left(\overline{w'\theta_l'}\right)}{\partial z} \tag{2.3}$$

$$\frac{\partial \overline{q_t}}{\partial t} + \overline{u}\frac{\partial \overline{q_t}}{\partial x} + \overline{v}\frac{\partial \overline{q_t}}{\partial y} + \overline{w}\frac{\partial \overline{q_t}}{\partial z} = \frac{S_{q_t}}{\overline{\rho}} - \frac{\partial\left(\overline{w'q_t'}\right)}{\partial z} \tag{2.4}$$

In these equations, phase changes are accounted for by using θ_l and q_t.

For equations (2.1-2.4) the first term on the left hand side (lhs) is a storage (or tendency) term. The other three terms on the lhs describe the horizontal advection and vertical advection, or subsidence. The first terms on the right hand side (rhs) of 2.1 and 2.2 represents a departure from the geostrophic winds. The last term on the rhs of all equations is the turbulent flux divergence term. The first term on the rhs of the heat equation is a radiative flux divergence term.

Summarized, the net temperature tendency is determined by the tendencies due to: *horizontal temperature advection*, *subsidence*, *radiative flux divergence* and the *turbulent heat flux divergence*. The net humidity tendency is determined by: *horizontal moisture advection*, *subsidence* and the *turbulent moisture flux divergence*.

Not taking into account the storage term and the flux divergence term, which depends on the turbulence on a scale smaller than the LES domain and which is explicitly calculated by LES, all the above terms are large-scale forcings. These forcings cannot be solved by LES as they occur on scales larger than the LES domain and thus have to be prescribed. The tendency equation of the horizontal average field of temperature for example is separated into the following two parts:

$$\frac{\partial \overline{\theta}_l}{\partial t} = \left(\frac{\partial \overline{\theta}_l}{\partial t}\right)_{forcing} + \left(\frac{\partial \overline{\theta}_l}{\partial t}\right)_{model} \tag{2.5}$$

in which the forcing term represents the tendency due to large-scale horizontal advection, subsidence and radiation and the second term is the turbulent flux divergence term calculated by LES:

$$\left(\frac{\partial \overline{\theta}_l}{\partial t}\right)_{model} = -\frac{\partial\left(\overline{w'\theta_l'}\right)}{\partial z} \tag{2.6}$$

In this study the DALES (Dutch Atmospheric LES) model version is used, which is tuned to shallow cumulus and perhaps even to the RICO case. This implies that the initialization

set needed for LES (discussed in the next section) is also tuned to the RICO precipitating cumulus case. Specific forcings and conditions need to be prescribed for this case, but certainly a different approach may be required in other studies and other model versions. Specifications of the turbulent schemes, condensation and advection schemes, time schemes and closures used in this version can be found in Cuijpers and Duynkerke (1993); Siebesma et al. (2003). Although the LES case is based on precipitating cumulus, the test simulations described in this study are performed with a LES version *without* microphysical schemes implemented, implying no precipitation is produced in any of the simulations.

2.1.2 The LES initialization set

A simulation with LES is initialized with a prescribed mean state of the atmosphere, from which the model will evolve during the simulation. For a marine boundary layer studied here the change in the vertical profiles of liquid water potential temperature and total specific humidity, is little. The prescribed surface fluxes determine the amount of heat, moisture and momentum that is available, but the flux divergence terms in for example Equation 2.6 depend on the turbulence solved by LES. During the simulation, the large-scale forcings, described in the previous section will determine together with the flux divergence term the net tendencies for temperature, humidity and the horizontal winds.

Summarized, the parameters and forcings in the LES initialization set that need to be estimated are:

Initial vertical profiles of:

- The liquid water potential temperature θ_l
- The total water specific humidity q_t
- The zonal and meridional wind speed u and v

Vertical profiles of the following large-scale forcings:

- The subsidence $\overline{w}_s$ in ms^{-1};
- The (liquid water) potential temperature tendency due to horizontal advection: in Ks^{-1};
- The specific humidity tendency due to horizontal advection: in $\mathrm{kgkg}^{-1}\mathrm{s}^{-1}$;
- The temperature tendency due to radiation in Ks^{-1};
- The geostrophic winds, u_g and v_g in ms^{-1}.

The subsidence w_s determines the temperature and moisture tendencies due to subsidence, which are calculated in LES, by combining this subsidence with the prescribed mean thermodynamic profiles.

Surface conditions

- Sea surface temperature (SST) in K;

- Surface heat and moisture flux (prescribed **or** parameterized);

- Roughness length z_0, friction velocity $u*$ or drag coefficients (prescribed **or** parameterized), which determine the momentum fluxes.

Several options exist in LES to specify the surface conditions. One can choose to either prescribe the surface fluxes or to parameterize them, in which case fluxes are calculated in LES itself and are continuously adjusted to the thermodynamic state of the lower atmosphere. This choice depends on whether confident estimates for these fluxes can be obtained from observations, but also on the degree of freedom that is desired for a certain simulation.

Among the initialization set for the LES case are the domain and simulation characteristics. The domain size and simulation characteristics of the final LES initialization set are given in Appendix C. These characteristics deviate at some points from the ones used in the test simulations. Unless mentioned otherwise, all test simulations discussed in this report are performed on a domain of 6400 x 6400 x 4000 m, and a resolution of 100 x 100 x 40 m. The time step of all simulations is 2 s and the duration 12 hours. The translational x- and y- speed components of the domain, cu and cv, are -6 and -4 ms^{-1}resp.

2.2 The RICO field study

2.2.1 General overview

The name 'Rain in Cumulus over the Ocean Experiment (RICO)' reveals its aim and objective immediately. Its general goal is to study the dynamics of shallow cumulus clouds in the trade wind regions, with a special attention to precipitation processes. The overall scientific goal of RICO is to understand and describe the characteristics of the trade-wind cumuli and all the processes involved, with special attention to precipitation processes.

The RICO field study took place from the 21^{st} of November (2004) to the 25^{th} of January (2005) in the region around the Caribbean islands of Antigua and Barbuda, see Figure 2.1(a), where trade-wind cumulus clouds frequently occur. Radar images of earlier studies have shown that precipitation is prevalent in this area during the winter months. This period was also chosen to avoid hurricanes, fronts and periods of deep convection. Most of the measurements were conducted upwind of the islands, in an area fully exposed to the undisturbed trade-winds (see Figure 2.1(b)).

During the first part of the experiment, in November and December of 2004, and the second part, January 2005, the (NCAR) S-PolKa radar located on the island of Barbuda performed measurements. This radar gathered rainfall statistics of an area with a radius up to 150 km. Other operations performed during the full RICO period included flight performed by the NCAR C-130 aircraft and the (University of Wyoming) King Air aircraft. In the second period, another research aircraft (the United Kingdom BAE-146) and one research vessel (RV Seward Johnson) were added to the RICO operations. A wide variety of instruments was carried on board of all aircrafts and the ship, including a dropsonde system, lidars, several (Doppler) cloud radars and instruments to measure basic atmospheric variables, basic cloud microphysics, trace gas chemistry, and detailed cloud and aerosol

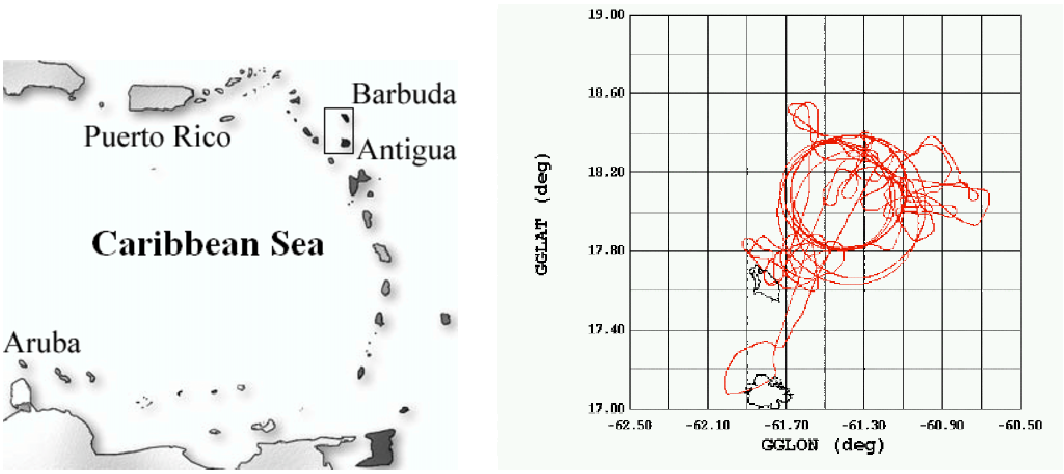

(a) The Caribbean with Antigua & Barbuda in rectangle box

(b) Example of a flight track of the NCAR C-130 in the research area NE of Barbuda

Figure 2.1: Research area of the RICO field study

properties. During the entire period, basic atmospheric variables were measured at a surface station located on Barbuda, from which also a set of 2-4 radiosondes were released each day (the Spanish Point radiosondes). Research flights were often conducted in an area NE of Barbuda (Figure 2.1(b)), where the research vessel was located as well.

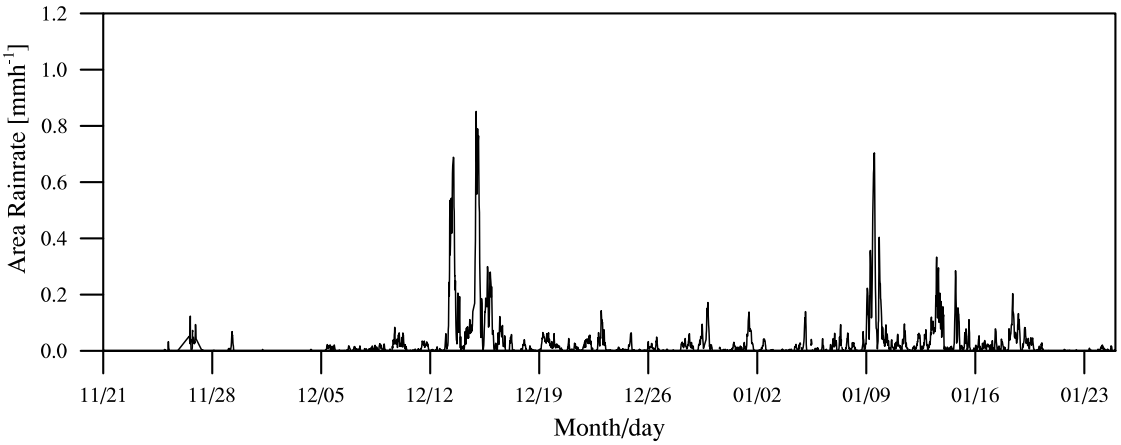

Figure 2.2: Area average rain rates in $mmh^{-1}$are plotted for the RICO operational period (month/day). Rain rates are derived from observations by the NCAR S-Pol radar located on Barbuda.

From the observations of the SPol radar, area rainfall estimates were obtained for the whole operational phase of the experiment (see Figure 2.2), showing that rainfall in the trades occurs frequently. Excluding some of the heavy rain events, on for example December 14^{th} and January 9^{th}, that are due to large-scale disturbances, many small rainpeaks are left, which are presumably associated with fields of trade wind cumuli. This rainfall time serie is shown in more detail in Appendix A, along with the operations that

were performed during the same period. This time serie has been used as a footprint to select days or periods during RICO suited for the LES case.

2.2.2 Selecting cases during RICO for LES

As mentioned already in the Introduction, several LES cases were considered. Depending on the variety of observations available for each day during RICO, several days were considered that are not only interesting for the LES modeling community, but also for other research groups focusing on microphysic or aerosol studies. Ideally the efforts of all research groups are combined, which can be achieved by focusing on the same case.

The 11^{th} of January (2005) is a day, on which a great variety of measurements was performed, giving the opportunity to compare LES results with real observations. Aircraft measurements were performed by the NCAR C-130 and the Whyoming King Air, and ship measurements were performed on this day as well. A reasonable amount of precipitation was observed on this day. The average area rainfall, estimated from the analysis of SPol radar observations, was about 0.6 mmd^{-1}, equivalent to 17 Wm^{-2}. This is also about the average amount of rainfall averaged over the whole RICO measurement period.

Initially we focused on this day for an LES case study. The available observations for this day were analyzed and evaluated. During the analysis, our focus shifted from January the 11^{th} to the three week period from December 16^{th} to January 8^{th}, hereafter called 'the supressed (composite) period'. This was due to difficulties in deriving the large-scale forcings for January 11 in combination with the observed thermodynamic structure on this day, which did not (yet) lead to satisfying LES results. This is discussed in more detail in the next chapter.

The supressed period of three weeks can be characterized as a typical trade-wind cumulus period with suppressed conditions and light, though prevalent, rainfall events. The period lies in between a few days with heavy rainfall events, see Figure 2.2. The average area rainfall during this period was about 0.34 mmd^{-1}, equivalent to 10 Wm^{-2}. Unfortunately, no ship measurements were performed during this period, and flight measurements are absent on most days except for the beginning and end of the period on which the NCAR C-130 and the Whyoming King Air performed measurements.

The thermodynamic state of the atmosphere can differ significantly between days or periods as observed from soundings. A short subjective analysis of the soundings showed that the mean state of the suppressed period is actually similar to that of a specific day within the period: Jan 7 2005 (C-130 research flight RF11). Thus there are still opportunitities to use observational analyses of this particular day for a comparison with the LES results in further studies.

Chapter 3

Analysis of RICO observations and a RACMO Hindcast

Observations and measurements performed during RICO were used as much as possible to construct reasonable large-scale forcings, initial thermodynamic profiles and surface conditions listed in section 2.1.2. The Regional Atmospheric Climate Model (RACMO) and two radiation schemes were used in addition. In the following sections we discuss the analysis of the RICO observations and a RACMO HindCast. Consequently we show the results for the case that is considered: the one based on the suppressed period with mostly trade wind cumuli. In addition at the end of this chapter we will also show a few results based on January 11 as a comparison. These results will further clarify our choice to first focus on the suppressed period.

3.1 Data analysis

3.1.1 RICO observations

Various sounding data obtained during RICO are available that can be used to construct initial thermodynamic profiles for LES. Among the sounding data are the radiosondes released from Spanish Point on Barbuda, typically 2 to 4 on each day during the RICO operational period. In addition, during each research flight of the NCAR C-130 aircraft, typically 10 to 16 dropsondes were released. The research vessel RV Seward Johnson released radiosondes as well, but only from January 3rd onwards and can thus not be used to construct profiles for the suppressed period.

Although for each flight day far more dropsondes than radiosondes are released, in total fewer dropsonde data are available. This is especially true for the suppressed period when just a few research flights were performed (Appendix A). However, the average profiles of Spanish Point and of the dropsondes during the suppressed period do not differ remarkably, except for the humidity values close to the surface, which are a bit larger for the dropsondes as compared to the Spanish Point (see Figure 3.1). This is not remarkable as dropsondes are released above sea instead above land.

Both types of sounding data are used to construct vertical profiles of temperature, humidity and winds of which the results are shown in section 3.2.

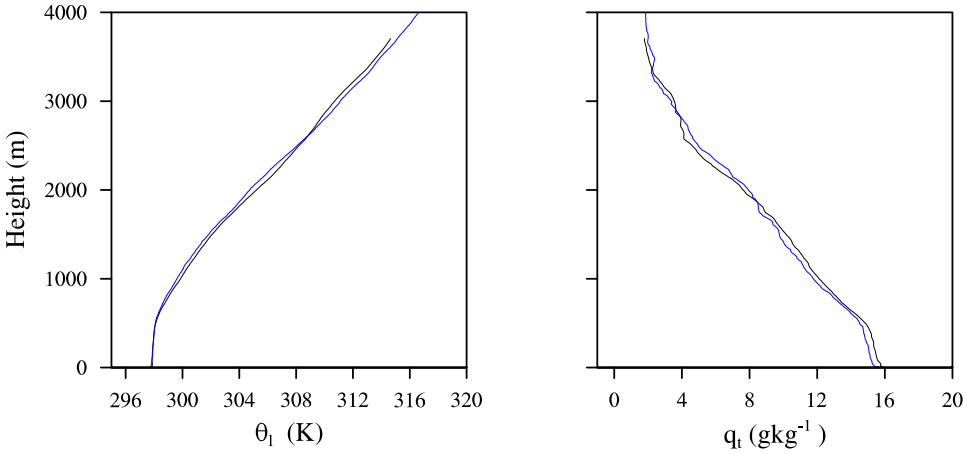

Figure 3.1: Vertical profiles are shown of (a) the potential temperature (K) and (b) the specific humidity (gkg^{-1}). The profiles are averages over the suppressed period. The dropsondes profiles are shown in black and the Spanish Point profiles in blue.

In previous LES cases aimed at studying shallow cumulus convection, large-scale forcings were derived from observations obtained during field studies. During BOMEX (Barbados Oceanographic and Meteorological Experiment) when mostly trade-wind cumuli were observed, an extensive dataset was obtained by launching rawinsondes from ships at each corner of a 500 x 500 km^2 square for every 1 1/2 h. Using this data, heat and moisture budget analyses were performed, leading to estimates of the large-scale advection and subsidence (Holland and Rasmusson, 1973) which have been used until now for LES studies. Unfortunately, such an analysis cannot be performed with the sounding data from RICO, because the soundings are only available at three (varying) locations and are not released frequently enough.

However, during the case set-up the following possibility was considered to derive large-scale advection and subsidence. The six circles flown by the aircraft on each flight day (each $\approx$ 60 km in diameter and at three different heights: close to the surface, at cloud base and in the free troposphere) can in theory be used to derive the divergence and advection on a mesoscale (Lenschow et al., 1999). It is known that in case not an exactly closed circular pattern is flown, it may be more complicated to derive accurate estimates. We performed a short study focusing on the derivation of large-scale advection from the cirles flown on January 11^{th} during RICO. By using the aircraft measurements of specific humidity and the horizontal winds (see also Holland and Rasmusson (1973)) we derived estimates of advection and divergence. Unfortunately this short analysis did not yet lead to reasonable estimates for the large scale advection of heat and moisture. More specific, divergence values were far too high and the advection profiles changed considerably with time (even with a change of sign). An extensive circle analysis however was beyond the scope of this study. This was also the reason that we did not explore the possibility of using dropsondes from the C130 to estimate the large scale advection. Instead, we turned towards the Regional Atmospheric Climate Model (RACMO) to derive estimates of the large-scale advection and subsidence.

3.1.2 A RACMO HindCast for the RICO area

A HindCast was performed with the Regional Atmospheric Climate Model (RACMO) for a total domain of 96 x 90 gridpoints with a resolution of 22 km. The domain was centered on the main RICO research domain where most research flights were performed (Figure 3.2). The HindCast was performed for a total period of two months (December 2004 and January 2005). RACMO is essentially a high-resolution limited area version of the ECMWF model and is initialized every 24 hours with the ECMWF analysis at 12 UTC. It makes a 36 hour forecast, from which the first 12 hours are considered to be a spin-up of the model and are consequently discarded. Combining the remaining 24 hours of each day results in a two month time serie with a time resolution of 10 minutes. Output of this HindCast was produced for a small subdomain (cenetered on 61.46W, 17.97N), consisting of 5 x 5 gridpoints thus comprising an area of $\approx$ 110 x 110 km^2. Output data is thus available at each of these 25 gridpoints and at each ECMWF pressure level (with the top level at about 30 km). All RACMO output variables are averaged over this subdomain.

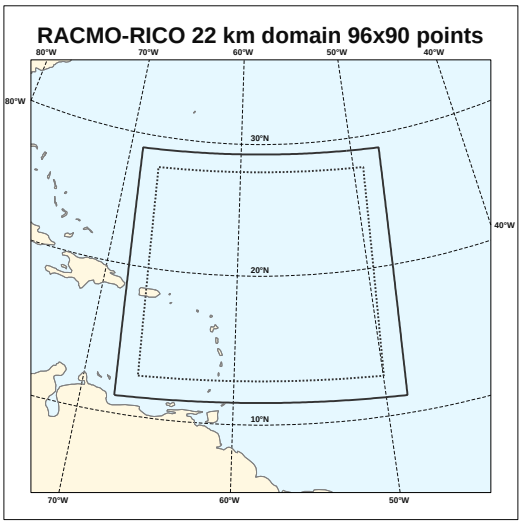

Figure 3.2: Domain of the RACMO HindCast centered on the RICO research area, northwest of the Caribbean islands Antigua and Barbuda, at 61.46W, 17.97N.

Among the RACMO output data that we use in this study the most important are: (1) the *total tendency due to horizontal and vertical advection*, (2) *the vertical velocity omega* ($\omega = dp/dt$) and (3) the *vertical profiles of temperature and humidity*. These variables are used to estimate large-scale advection and subsidence. The subsidence w_s is derived from the vertical velocity omega ω (2) and determines the temperature and moisture tendencies due to subsidence. The tendencies due to solely horizontal advection, are derived as follows: Combining ω (2) and vertical profiles (3), one can derive the tendency solely due to subsidence. Subsequently, from the total tendency (1) and the just derived tendency due to subsidence, the tendency due to solely horizontal advection can be derived. These methods are described in more detail in Appendix B.

3.1.2.1 RACMO versus RICO observations

The vertical profiles of potential temperature θ and specific humidity q_T and a time series of convective precipitation are used to consider the level of agreement between RACMO results and RICO observations. The pattern of the convective rainfall from RACMO [1], which is shown in Figure 3.3, coincides to a reasonable level with SPol rainfall observations (shown in Figure 2.2). The relatively dry period in between the heavy rain events, previously defined as trade-wind cumulus 'suppressed' period (04/12/16 - 05/01/08), is also a clear feature in the RACMO time series. The profiles of θ) and q_T, which are averages of the suppressed period, are compared with the average profiles of the soundings released from Spanish Point (see Figure 3.4). On average RICO observations show a somewhat cooler and more humid atmosphere than RACMO. This is in agreement with the surface fluxes produced by RACMO, which are on average higher than the ones observed during RICO (see section 3.3). In RACMO the conversion of cloud liquid water to precipitation (rain water) occurs immediately as clouds develop, which is probably leading to heavier precipitation as shown in Figure 3.3 and thus depletion of moisture.

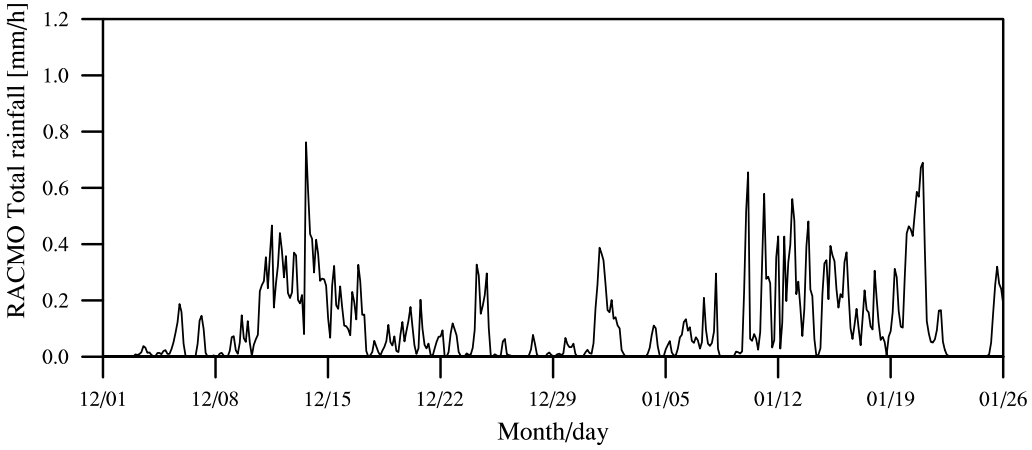

Figure 3.3: Total rainfall in mmh^{-1}at the surface from the RACMO HindCast. Rain rates are averages of the RICO subdomain (see Figure 3.2).

3.1.3 Radiative transfer schemes

Another forcing that needs to be prescribed for LES is the temperature tendency due to radiation. As all other forcings, we like to prescribe a radiative forcing that accounts for both day and night and thus represents an average forcing over 24 hours. Two radiative transfer schemes were consulted to estimate this forcing: the MODTRAN and ECMWF radiative transfer schemes. Both schemes use an assumed climatology for aerosols and their absorption and scattering coefficients, ozone and other atmospheric constituents/gases. The input parameters for these models are the vertical distribution of relative humidity

[1] Convective precipitation is yet produced in RACMO when a minimum cloud depth of 0 m is exceeded, and one can thus expect precipitation to be overestimated.

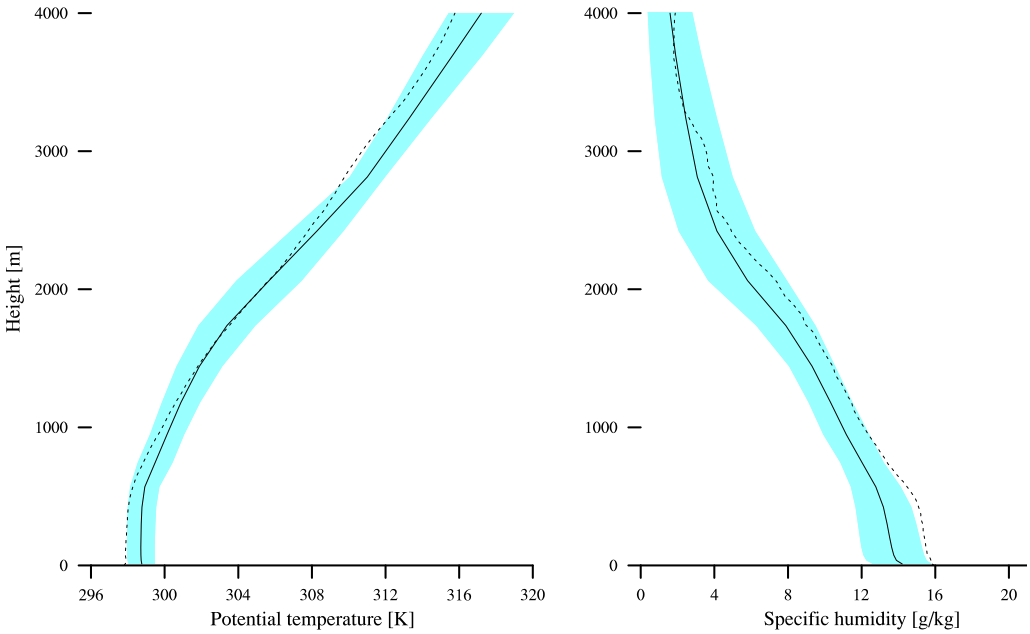

Figure 3.4: Vertical profiles of potential temperature (K) and specific humidity (gkg^{-1}) are shown for the lowest 4 km of the atmosphere (the vertical domain size prescribed in the current LES case). As a black line the average profiles of RACMO are plotted for the period 04/12/16 - 05/01/08, with in light blue ± one standard deviation. The dotted black line represents the average of all soundings from Spanish Point during that same period.

and temperature up to a level of about 40 mbar, as well as the latitude and longitude and the surface temperature. To provide this input, again sounding data from RICO was used.

The input profiles for the radiation models have been constructed by taking the average dropsonde profiles up to a level of about 600 mbar (the maximum level at which dropsonde data is available) and extending that profile with average Spanish Point sounding data up to a level of 44 mbar. It was manually checked if the different sounding profiles at 600 mb connected well. An average sea surface temperature (SST) was derived from RACMO output. Profiles were constructed for both January 11 and the suppressed period.

The MODTRAN scheme was initialized with average profiles for January 11 and assumed clear-sky conditions (a reasonable assumption considering the low cloud-cover of shallow cumulus). The ECMWF radiation scheme was initialized with average profiles for the full suppressed period, also assuming clear-sky conditions.

3.2 Results

3.2.1 The suppressed period (Dec 16 - Jan 08)

3.2.1.1 Vertical profiles of temperature, humidity and winds

The average Spanish Point soundings of the suppressed period are shown in Figure 3.5 as black lines with one standard deviation indicated with the grey band. Vertical profiles are shown for temperature, humidity and the horizontal winds. The dotted black line in

the plot for specific humidity represents the saturation specific humidity. It is difficult to distinguish an inversion, which may be due to averaging profiles over the suppressed period. If one compares these profiles to the classic BOMEX cases (for example Siebesma and Cuijpers (1995); Siebesma et al. (2003)), the cloud layer observed during RICO appears to be a bit more stable, and the inversion slightly more unstable.

The initial profiles for LES constructed from these profiles of the suppressed period are shown as red lines in 3.5. These profiles are based on Spanish Point, except for the humidity values close to the surface which are based on the dropsondes profiles. The latter show a slightly higher humidity close to the surface.The exact specification of the prescribed LES profiles for the composite case are given in Appendix C as part of the final initialization set.

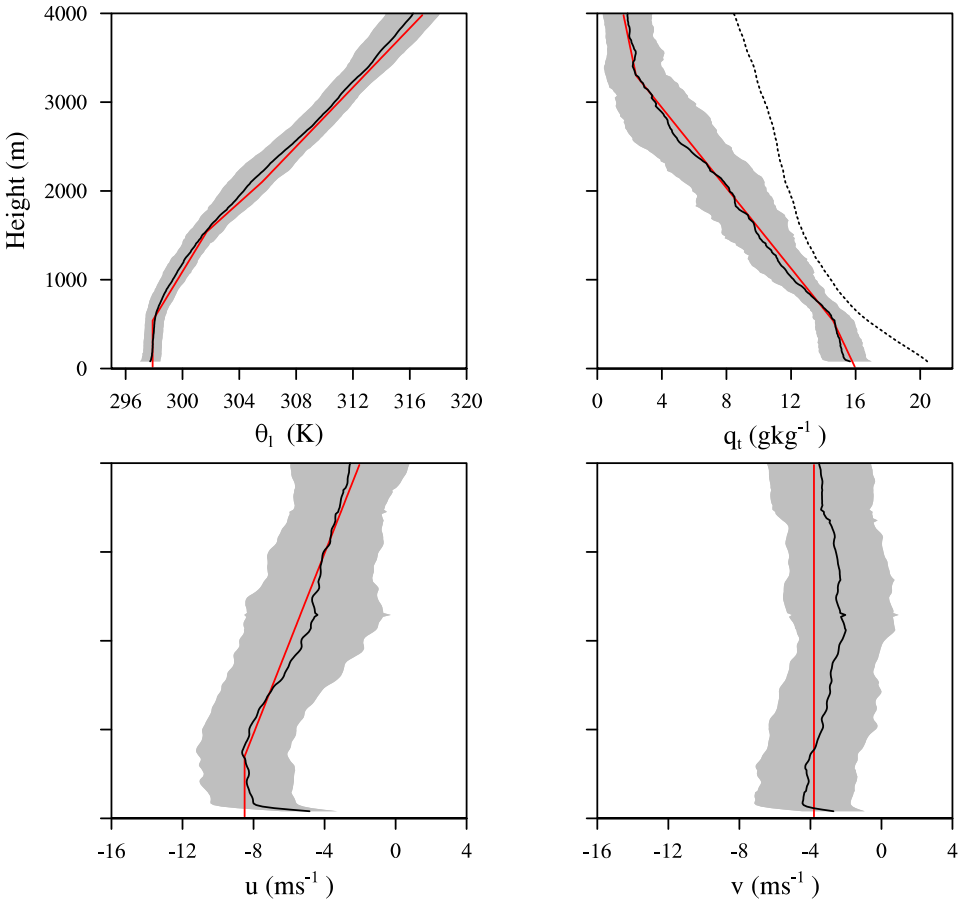

Figure 3.5: Vertical profiles are shown of (a) the potential temperature (K), (b) the specific humidity (gkg^{-1}), (c) the zonal wind (m/s) and (d) the meridional wind (m/s). As solid black lines the mean profiles of the suppressed period are shown with in grey $\pm\sigma$. The dotted lines represent the saturation specific humidity (gkg^{-1}). In red the profiles as constructed for LES are shown.

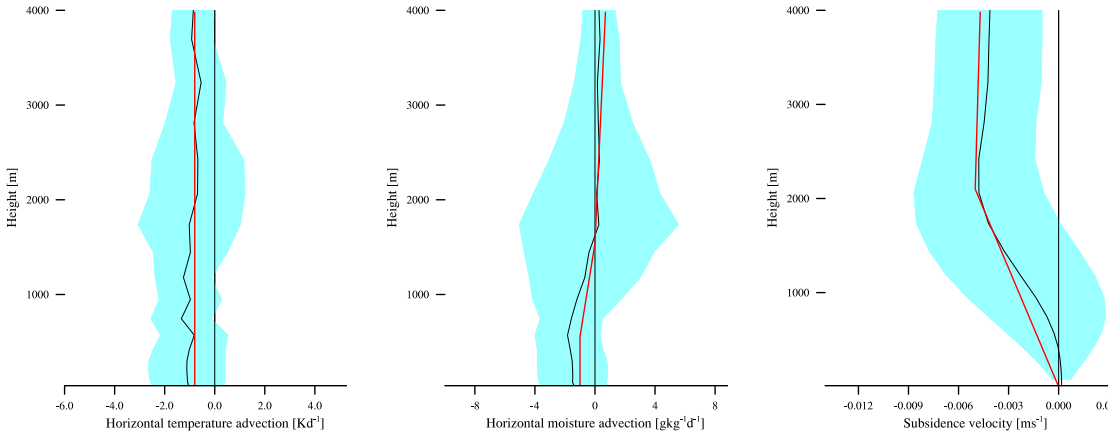

(a) (b) (c)

Figure 3.6: The spatial and temporal average RACMO profiles of (a) the temperature tendency due to horizontal advection, (b) the moisture tendency due to horizontal advection and (c) the subsidence are plotted for the suppressed period (as black solid lines with in light blue $\pm 1/2\sigma$). The solid red line represents the LES profiles constructed from these RACMO profiles for the suppressed period.

3.2.1.2 Large-scale forcings

Mean vertical profiles of the horizontal moisture and (potential) temperature advection and the subsidence are calculated using the RACMO HindCast and plotted in Figure 3.6. In black the average profile of the suppressed period is shown, along with a light blue band of $\pm 1/2$ a standard deviation. In the lower atmosphere (0 - 4 km) horizontal advection for the suppressed period on average results in cooling throughout the whole layer, a drying of in the lowest 2 km and a small amount of moistening in the upper 2 km. Subsidence is present in the whole layer and increases with height, which ensures the warming and drying in the boundary layer needed to balance the tendencies due to turbulent flux divergence, radiative cooling and advection. The profiles constructed from these results which we prescribe for the LES case are also plotted in Figure 3.6 as red lines. The exact specification of these profiles for the LES case can be found in Appendix C.

Temperature tendencies due to large-scale horizontal advection were also estimated from the thermal wind relationships as a comparison *i.e.*, by using horizontal winds and large-scale temperature gradients (see also Appendix B). Rough estimates for the horizontal temperature advection typically give a cooling of about 0.8 - 0.9 Kd^{-1}, which is in accordance with the mean values derived from RACMO.

3.2.1.3 Radiative cooling profile

A vertical profile of the temperature tendency due to radiation is shown in Figure 3.7. This profile represents a daily average profile, produced with the ECMWF radiative transfer scheme. This figure illustrates a cooling rate of about 3 Kd^{-1} at the surface, decreasing to 1 Kd^{-1} at a height of 3 km, above which it slightly increases again. From this profile a

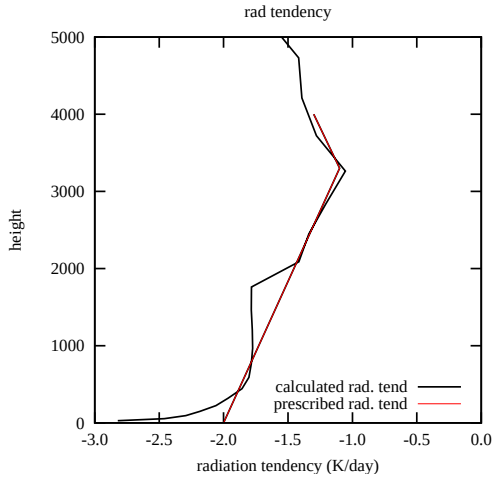

Figure 3.7: Temperature tendency (Kd^{-1}) due to radiation from an offline ECMWF radiation scheme. Profiles are based on the average suppressed soundings. The profile shown is averaged over 24 hours. In red the prescribed LES profile is shown.

radiative cooling profile for LES was constructed. The LES profile is showed as a red line in Figure 3.7. The main difference between the original and prescribed LES profile is the cooling rate at the surface, which is minimalized to 2 Kd^{-1} for LES.

From the average profiles of the horizontal winds above the mixed-layer the two components of the geostrophic wind (u_g, v_g) are constructed. Since the LES initial profile of the meridional wind has a zero lapse rate at each level, the y-component of the geostrophic wind is equal to the meridional wind. The lapse rate of the zonal wind above 700 m is used as the lapse rate of the x-component of the geostrophic wind and interpolated to the surface. The exact specification of the geostrophic winds is found in Appendix C.

3.2.1.4 Surface conditions

Measurements of surface heat and moisture fluxes have been performed by R/V Seward Johnson but only during the period of January 9 - 25. Therefore other sources were consulted to obtain surface flux estimates for the suppressed period. Surface fluxes from the RACMO HindCast, available for the two months December and January, were compared to the ship measurements. This is shown in Figure 3.8. The flux values from these two sources coincide well during the overlapping month January, however, it is evident that RACMO fluxes are on average higher than the fluxes measured by the ship. The lower values for the specific humidities in RACMO, shown previously in Figure 3.4, may explain the higher surface fluxes in RACMO.

A quick analysis of the average moisture fluxes from aircraft measurements performed at the lowest flight circles (approximately 70 m above the sea surface), showed that fluxes during the suppressed period can vary from 100 $Wm^{-2}$to 200 Wm^{-2}, thus showing quite some variability.

For this case, we have chosen to parameterize fluxes in LES instead of prescribing them, since we are unsure about the exact magnitude of the fluxes during the suppressed period.

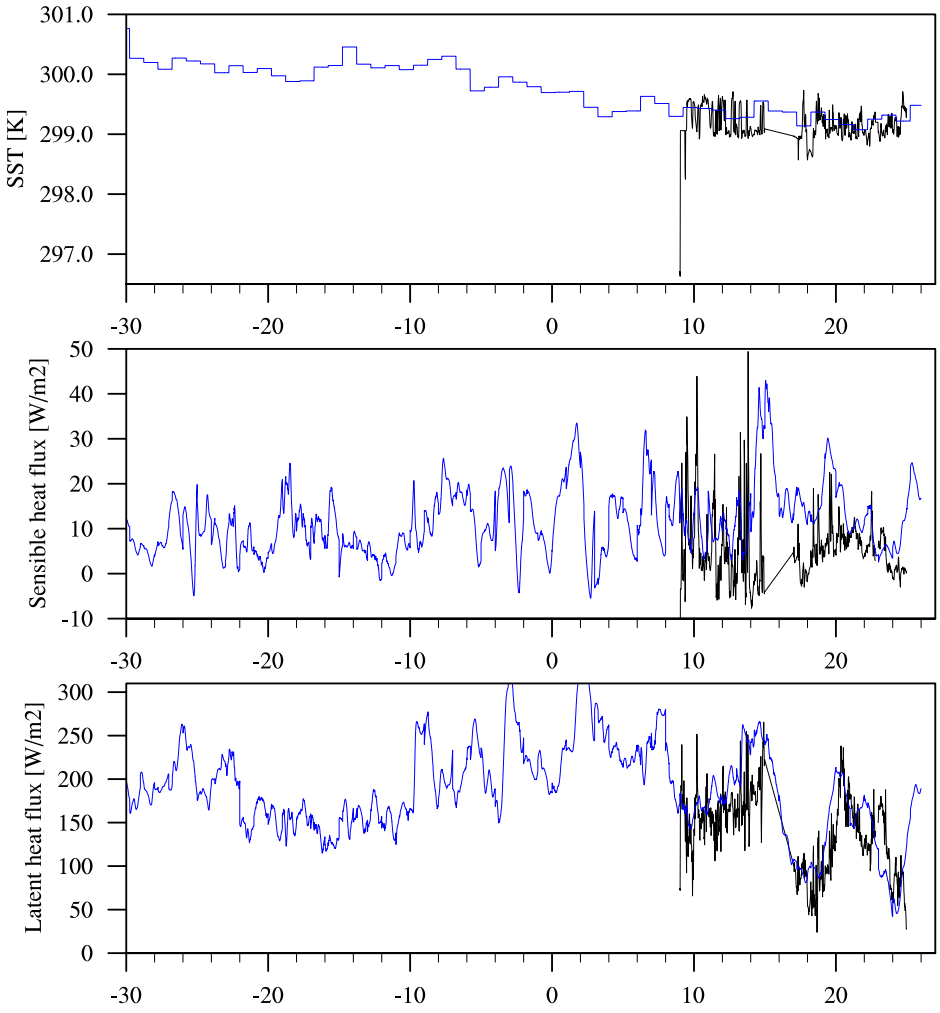

Figure 3.8: The sea surface temperature (K), the sensible heat flux and the latent heat flux (Wm^{-2}) as measured by the RV Seward Johnson are shown in black against Julian Day. These measurements are only available for the ship operational period. In blue the results of the RACMO HindCast are shown, as averages for the 110 x 110 km^2 subdomain.

This leads to the additional advantage of a better budget closure for the subcloud layer, because the fluxes respond fast to the specified large-scale forcings. Therefore a SST needs to be specified. The SST from RACMO, averaged for the ship measurement period (top plot in Figure 3.8), is only slightly higher than the average SST measured by the ship. Since the SST in RACMO is based on global satellite observations we are quite confident about these values. The average SST during the suppressed period from RACMO is 299.8 K.

Other surface parameters obtained from RACMO are the roughness length z_0 or the friction velocity $u*$, from which the momentum fluxes are calculated. These two paramters are related by the empirical Charnock relationship, given by: $z_0 = 0.015 \cdot u^{*2}/g$ in which g is the gravitational acceleration. A value of 0.34 $ms^{-1}$for $u*$ results from averaging the $u*$ of the RACMO HindCast output over the suppressed period. This leads to an estimate of 1.6

10^{-4} for z_0, which is consequently converted to surface drag coefficients for momentum, heat and moisture ($C_m = 0.001229$, $C_h = 0.001094$ and $C_q = 0.001133$) which are prescribed for the final LES case.

3.2.2 January 11

The Spanish Point soundings for January 11 are shown in Figure 3.9. These soundings are released at 06, 12, 18 and 24 h local time. Considering these profiles as compared to this suppressed period, the main difference is the humidity in the cloud layer, inversion and free atmosphere. The specific humidity on this one day is about 1 - 3 g/kg larger at these levels than during the suppressed period. No strong inversion is observed. One of our reasons to shift our focus to an average three week case, is the variability observed in these thermodynamic profiles and in the time serie of rainfall on January 11 (Figure 3.10). Significant drying occurred in the upper layers during the morning, and moistening was present during the remainder of the day, of which mostly in the subcloud layer. During the night and early morning, rainfall occurred frequently, but during the afternoon and evening, hardly any rain is observed. These observations raised some questions reagrding whether such variability should be and can be simulated with LES. Consequently it came to mind to first simulate and understand the mean state of the three week, more suppressed and less variable period.

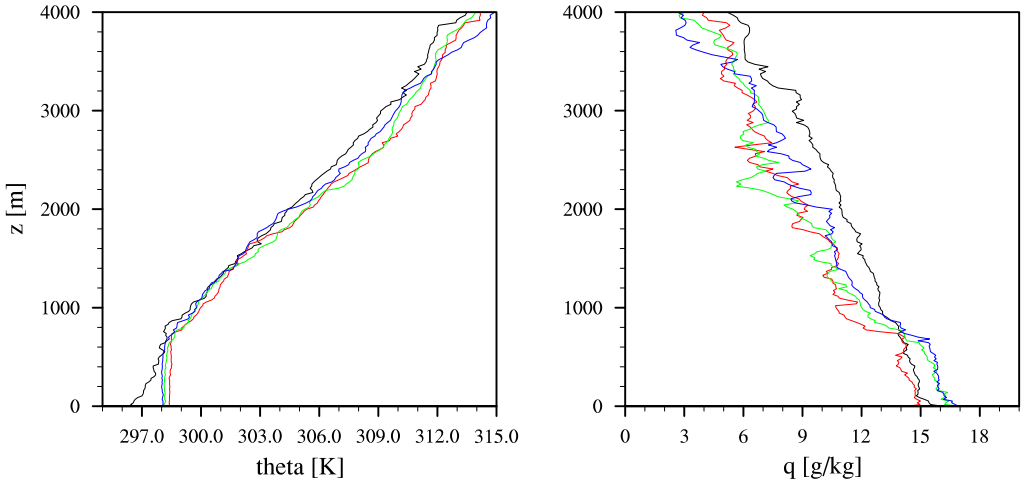

Figure 3.9: Vertical profiles are shown of the potential temperature (K) and the specific humidity (gkg^{-1}) from Spanish Point soundings. The colors black, red, green and blue represent soundings released at 11 (06), 17 (12), 23 (18) and 5 (24) UTC (local time in h) respectively.

A second reason to choose for this case were some issues in deriving the large-scale forcings for January 11. Using RACMO HindCast data and results from the MODTRAN radiative transfer scheme, large-scale forcings were derived and shown in Figure 3.11 and 3.12.

In general the profiles for January 11 are less smooth and obvious than the ones of the suppressed period. The temperature advection is near zero and the subsidence is positive at the lowest levels and has small values in general. The radiative cooling profiles shown

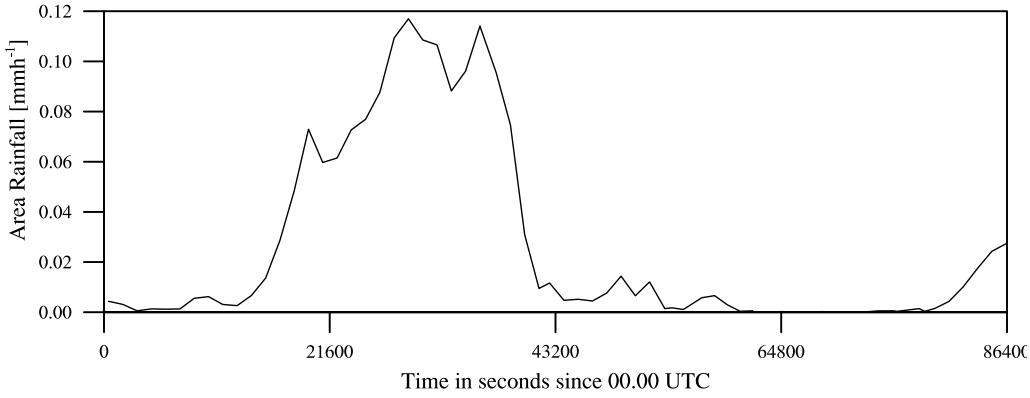

Figure 3.10: Area rainfall observed with the SPol radar during January 11 (UTC).

in Figure 3.12 are 12 hour average and daily (24-hour) average profiles of the temperature tendency. The 24 hour average profile illustrates a radiative cooling rate of about 4.5 Kd^{-1} at the surface, which decreases strongly to about 2 Kd^{-1} at levels above 500 m. The cooling rates of the 12 hour average profile are approximately half of those of the daily cooling rates. The daily average cooling rates in particular are quite large, resulting in a cooling excess especially at the upper levels. (We must note here that other estimates may be obtained by also running the ECMWF scheme with the January 11 profiles, however we only consulted the ECMWF scheme at a later stage during our studies when our focus was already on the suppressed period.)

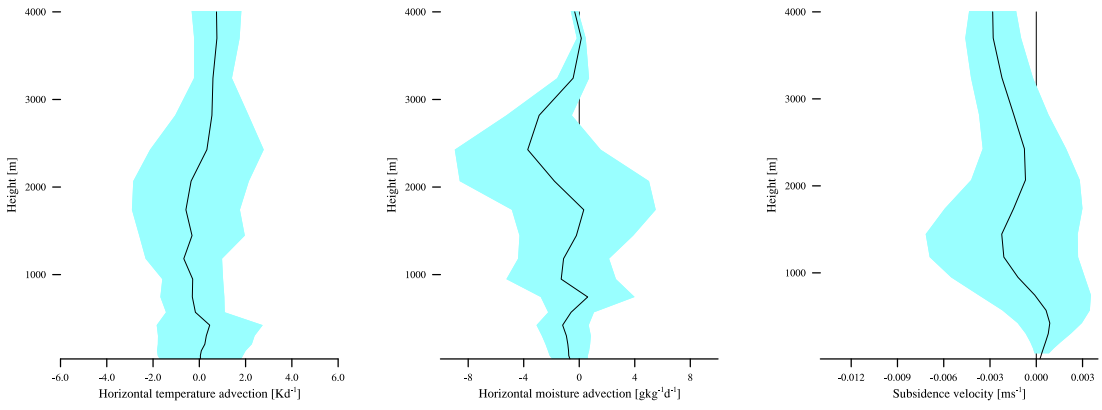

(a) (b) (c)

Figure 3.11: The spatial and temporal average RACMO profiles of (a) the temperature tendency due to horizontal advection, (b) the moisture tendency due to horizontal advection and (c) the subsidence are plotted for Jan 11 (as black solid lines with in light blue $\pm 1/2\sigma$).

The subsidence profile derived from RACMO in Figure 3.11(c) cannot compensate the strong radiative cooling shown in Figure 3.12. A quick calculation using an estimate of the subsidence rate at a height of 3 km ($w \approx 0.0015$ ms^{-1}) and a rough temperature gradient from Figure 3.9 at the same height ($d\theta/dz \approx 0.004$ Km^{-1}), results in a warming of about

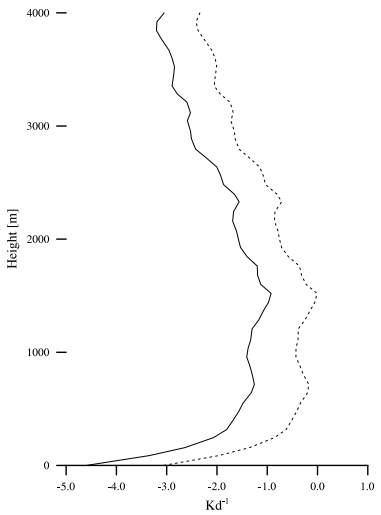

Figure 3.12: Temperature tendency (Kd^{-1}) due to radiation from the MODTRAN radiation scheme, based on the average Jan 11 soundings. The solid line is averaged over 24 hours, the dotted line over 12 (sunshine) hours.

0.5 Kd^{-1}. This is significantly smaller than the cooling of 2.5 Kd^{-1} shown in 3.12.

Since we had more confidence in the average large-scale forcings from RACMO for the three week suppressed period, we only performed LES runs combining the thermodynamic profiles of January 11 (in Figure 3.9) with the large-scale forcings of the suppressed period (Figure 3.6). These runs resulted in very deep clouds and a cloud cover exceeding 20 percent during most of the simulation. Since our focus had already shifted to the suppressed period, we did not continue to set up a LES case in much more detail based on this single day. Therefore it should be noted again that more analysis of January 11 may lead to large-scale forcings which do result in a mean state of LES that is close to the observations.

Chapter 4

Budget analysis and LES results

A budget analysis was performed to help construct the large-scale forcings for the LES case for the suppressed period. For the suppressed period considered, the storage term in the budget equations is expected to be little. Ideally the tendencies due to large-scale forcings are therefore in balance at each vertical level in LES, but at least the vertically integrated tendencies should balance each other such that the sum of these tendencies *i.e.*, the storage term, is close to zero. The budget analysis described here also further motivates our choice to construct the specific red vertical profiles of horizontal advection, subsidence and radiation (the prescribed LES profiles) shown in Figure 3.6(a) and 3.6(b), 3.6(c) and 3.7 in the previous chapter.

Estimates of the vertical integrated budget terms are derived in this chapter to get a feeling of the contribution of the different forcings. Some LES results of the final initialization set are shown and used to determine whether the prescribed forcings also result in a balance at different vertical levels.

4.1 Estimation of the heat and moisture budget terms

The tendency terms in the conservation equations for θ_l and q_t in Chapter 2 can also be written as vertically integrated budget terms in $\mathrm{Wm^{-2}}$. This is done by integrating any tendency from 0 to 4 km as follows:

$$\left\langle \frac{\partial \overline{\theta}_l}{\partial t} \right\rangle = \int \left(\left(\frac{\partial \overline{\theta}_l}{\partial t} \right)_z C_p \overline{\rho}_z \right) dz \tag{4.1}$$

$$\left\langle \frac{\partial \overline{q}_t}{\partial t} \right\rangle = \int \left(\left(\frac{\partial \overline{q}_t}{\partial t} \right)_z L_v \overline{\rho}_z \right) dz \tag{4.2}$$

in which the heat and moisture tendencies in $\mathrm{Ks^{-1}}$ and $\mathrm{kgkg^{-1}s^{-1}}$ are multiplied with the mean air density $\overline{\rho}$ ($\mathrm{kgm^{-3}}$) at each level, and with C_p or L_v ($C_p = 1004$ $\mathrm{Jkg^{-1}K^{-1}}$ and $L_v = 2.5\ 10^6 \mathrm{Jkg^{-1}}$).

This is done for all the tendencies in Equation 2.3 and 2.4 giving the following budgets for heat and moisture:

$$\left\langle \frac{\partial \overline{\theta}_l}{\partial t} \right\rangle_{storage} \approx \left\langle \frac{\partial \overline{\theta}_l}{\partial t} \right\rangle_{hor.advection} + \left\langle \frac{\partial \overline{\theta}_l}{\partial t} \right\rangle_{subsidence} + \left\langle \frac{\partial \overline{\theta}_l}{\partial t} \right\rangle_{radiation} + SH + P \quad (4.3)$$

$$\left\langle \frac{\partial \overline{q}_t}{\partial t} \right\rangle_{storage} \approx \left\langle \frac{\partial \overline{q}_t}{\partial t} \right\rangle_{hor.advection} + \left\langle \frac{\partial \overline{q}_t}{\partial t} \right\rangle_{subsidence} + LH - P \quad (4.4)$$

in which the vertically integrated flux divergence terms are replaced with the surface heat flux SH and surface moisture flux LH. Here we have included an extra term P for precipitation, which is a source for the heat budget and a sink for the moisture budget.

Some of these terms can be estimated without running a simulation in LES. The radiation term for example depend on the profiles that we construct and prescribe for LES. Other terms partly depend on the results from LES. For example the subsidence term depends on the vertical thermodynamic profiles to which LES evolves, because only the subsidence is prescribed. If the surface fluxes are parameterized, then their values depend on the cloud field produced in LES. The precipitation term also depends on this cloud field.

Nevertheless, a first guess of the budgets was made by estimating the different terms from the *initial* profiles and forcings and observations:

- The *advection* term: the red LES profiles for horizontal heat and moisture advection in Figure 3.6(a) and 3.6(b) are vertically integrated.
- The *subsidence* term: the red LES profiles for the subsidence (Figure 3.6(c)) and θ_l and q_t (Figure 3.5) are used to derive the tendencies due to subsidence $w_s\,(d\theta_l/dz)$ and $w_s\,(dq_t/dz)$, which are consequently vertically integrated.
- The *radiation* term: the red LES profile of the radiative cooling (Figure 3.7)) is vertically integrated.
- The *surface fluxes* term: since no ship measurements are available for the suppressed period, the available measurements during the ship operational period (January 9 - 25) are used. For this period the average SH $\approx$ 5 Wm^{-2}and the average LH $\approx$ 140 Wm^{-2}. These values are probably on the lower side.
- The *precipitation* term: the area rainrates derived from the SPol radar are used to calculate an average rainrate for the suppressed period, which is $\approx$ 0.34 mmd^{-1} or 10 Wm^{-2}.

Estimates of these terms were calculated for different LES profiles *i.e.*, the red profiles were continuously adjusted and the budget terms recalculated to derive at the best closure. Please note that this budget analysis remains a simplified analysis. Since we are quite confident about the profile of the subsidence that was obtained from RACMO, the subsidence profile was kept fixed. The radiative cooling term based on a 12 hour (sunshine hours) average profile instead of a 24 hour average profile, resulted in a smaller cooling term, which led to a better closure. However, since this case is based on the mean state of the atmosphere during the suppressed period, all forcings and initial profiles should be

averages over both day and night. And to be consistent, this also counts for the radiative cooling. Yet, the only profiles to play around with are the profiles of the tendencies due to horizontal advection. As seen from (Figure 3.6(a), 3.6(b)), these tendencies were slightly decreased as compared to the mean RACMO profiles, so that not too much cooling and drying was prescribed.
Taking the final LES profiles, the integrated tendencies (in Wm^{-2}) are as follows:

$$-15 \approx -36 + 75 - 69 + 5 + 10 \tag{4.5}$$

$$-6 \approx -11 - 125 + 140 - 10 \tag{4.6}$$

that lead to storage terms of -15 and -6 $Wm^{-2}$for heat and moisture respectively. These values roughly correspond to a temperature tendency of -0.3 Kd^{-1} for the entire colomn (0 to 4 km), and a moisture tendency of 0.05 $gkg^{-1}d^{-1}$, which are not unacceptable values.

Using parameterized fluxes will have a positive effect on the budget, as LES will respond to the prescribed cooling and drying due to advection by increasing the surface fluxes. Using 24-hour average cooling profiles has a considerable impact on the budget *i.e.*, yet there is more cooling than warming. In section 4.2.3, in which we show the LES results, we can see that this extra cooling is not positively influencing the strong cooling that is present in the cloud and inversion layer. One could consider to adjust the advection profiles such that at all heights a perfect balance between all forcings would be obtained. However, one can argue that by doing so LES is manipulated too much to conform to the user's expectations. Also, adjusting the moisture advection profiles in case of too much moistening at lower levels, by for example creating more drying, leads to the opposite effect. That is, the turbulent moisture flux responds to this increased drying and consequently causes even more moistening. For these reasons we did not further deviate from the RACMO derived profiles.

4.2 LES results for the final initialization set

The LES results shown in this section are based on the final initialization set that is summarized in Appendix C. The simulations performed are *without* microphysical processes included, thus precipitation cannot be produced.

4.2.1 Vertical profiles

The vertical profiles of temperature and humidity, liquid water, cloud cover, the horizontal wind components and the turbulent heat and moisture flux and buoyancy flux are shown in Figure 4.1. Cloud cover is defined as the number of cloudy gridpoints divided by the number of total gridpoints at each vertical level. Each horizontal mean profile is averaged over one hour. The duration of the simulation was 12 hours, from which the first two hours are considered spin-up time, and thus 10 profiles are shown for each variable.

The profiles of θ_l and q_t show that even after 12 hours of simulation the cloud layer and inversion layer are still cooling and moistening, due to the evaporation of cloud liquid water. The cloud layer is still deepening and getting slightly more unstable. Compared to

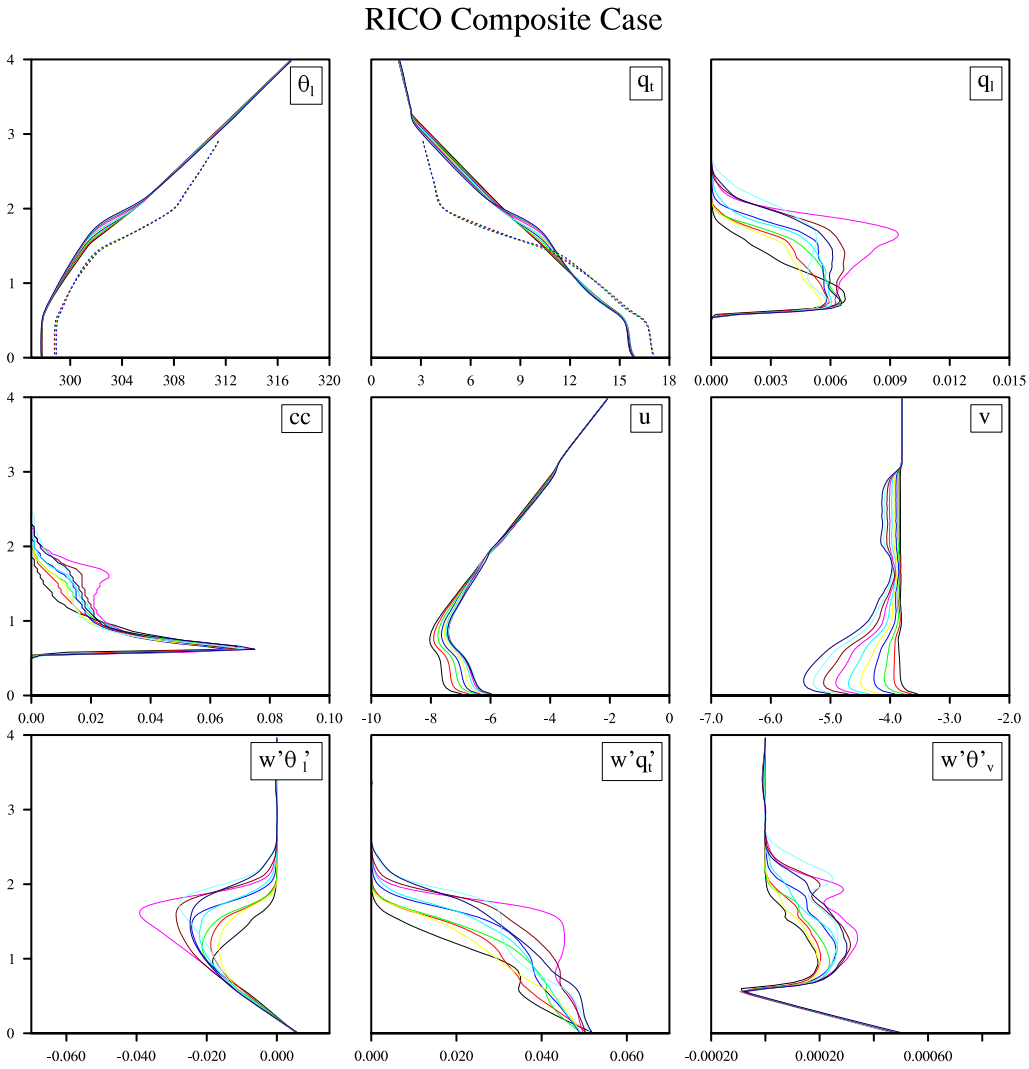

Figure 4.1: Horizontal-mean profiles of basic variables from a LES run performed with the final initialization set for the precipitating cumulus case (Appendix C). From left to right, top to bottom are shown: liquid water potential temperature (K), liquid water content (gkg^{-1}), total water specific humidity (gkg^{-1}), cloud cover (-), zonal wind speed (ms^{-1}), meridional wind speed (ms^{-1}), turbulent θ_l temperature flux (Kms^{-1}), turbulent q_t flux ($gkg^{-1}ms^{-1}$) and the buoyancy flux (Kms^{-1}). Each profile is averaged over one hour. The first two hours of the simulation are not shown. In dotted lines the BOMEX profiles are shown (Siebesma et al., 2003).

the previous BOMEX intercomparison case ((Siebesma et al., 2003) these clouds are more vigorous. Worth mentioning is the cloud liquid water profile: during the 8^{th} hour of the simulation (the pink line) the average cloud liquid water does not decrease above cloud base, but is reaching a maximum at much higher levels, with an associated increase in cloud cover. It is seen from the flux profiles that this increase is associated with an increase of water vapor transport into the inversion, leading to high tendencies and strong moistening and cooling. Opposite to the initial profile of temperature, these profiles do show an

inversion that is even getting stronger with each hour that passes by. The temperature gradients in both cloud layer and inversion layer seem to evolve to the same gradients as observed in the BOMEX case. LES is very sensitive to the gradient in these layers. From test simulations it is seen that if an initial profile with a very unstable cloud layer is chosen, the cloud activity in LES tends to stabilize this layer, instead of destabilizing it as we observe here.

Despite the ongoing changes in the profiles at the cloud and inversion layer, the forcings are in good balance and one may speak of a steady-state. The steady state in the subcloud and cloud layer is also due to the parameterized fluxes, which respond to changes in the subcloud layer. When viewing the temperature profile the subsidence and the radiation forcings in the free troposphere seem to be in a good balance. The humidity profile does however show a considerable drying at the lower levels of the free atmosphere, but it is not very likely that this inbalance affects the development of the cloud field too much. The profiles of the horizontal wind evolve as expected from the prescribed geostrophic winds.

4.2.2 Time series

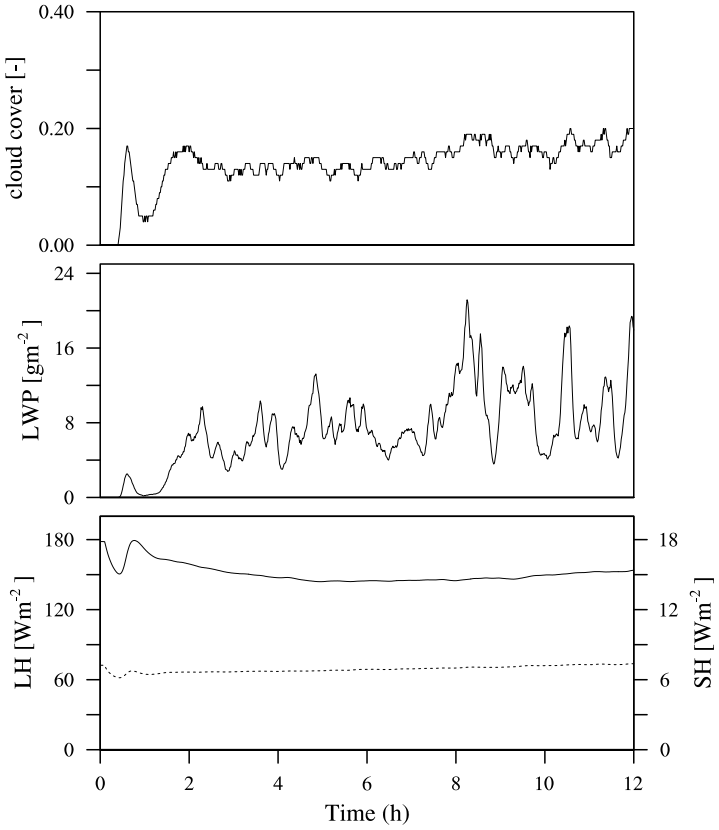

Figure 4.2: A time serie is shown of (from top to bottom): the cloud cover (-), the vertically integrated liquid water path (gm^{-2}) and the surface heat flux (dotted line) and latent heat flux (solid line) in Wm^{-2}.

A time serie for 12 hour of simulation is shown in Figure 4.2. The time evolution is

shown for the total cloud cover, the liquid water path and the surface fluxes. It is evident that the first two hours are a spin-up of the model. A typical cloud cover in the next few simulation hours is about 15 %, and in the last few hours this increases to about 18%. Large variations in the liquid water path are seen. The surface fluxes are plotted in addition as these are parameterized in LES. At the start of the simulations, the latent heat flux is high, reaching 180 Wm^{-2}, but during the simulation it steadily decreases to 150 Wm^{-2}. The heat flux shows smaller changes. After a small dip during the spin-up, it increases with very small values to reach a flux of 7 Wm^{-2}at the end of the simulation. This very small change in heat flux is in agreement with the vertical profile of temperature in the subcloud layer that does not show many changes either. Although difficult to see from the humidity profile, a little moistening is present in the subcloud layer, which may explain the smaller latent heat flux.

4.2.3 Tendencies due to large-scale forcings and turbulent fluxes

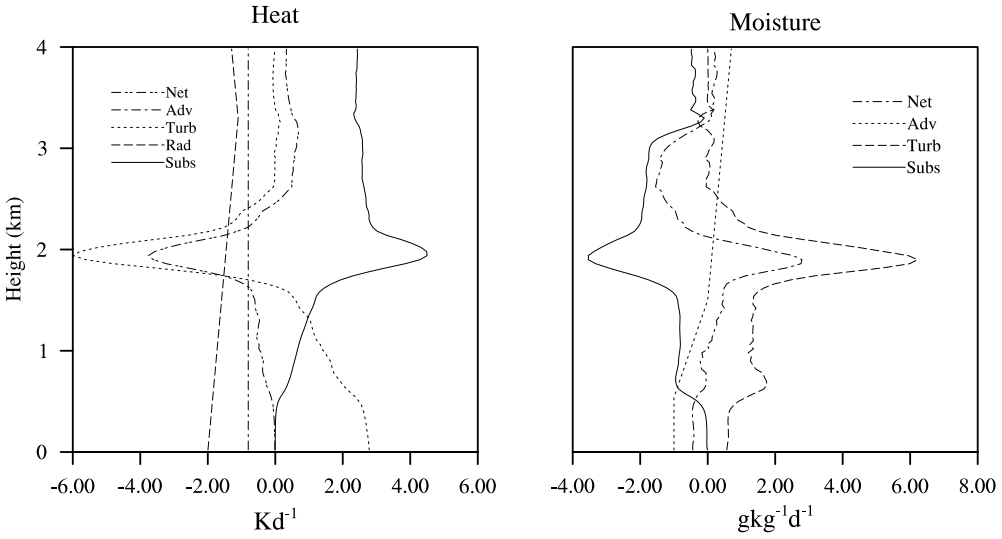

Figure 4.3: Vertical profiles of all forcings are plotted for heat and moisture. The tendencies are averages of the last three hours of the LES simulation. Adv = advection, Turb = turbulent flux divergence, Rad = radiative forcing, Subs = subsidence, Net = the sum of all terms (ignoring precipitation).

The budget analysis shown in section 4.1 is based on estimates and *initial* vertical profiles, and mainly used as a guideline to construct reasonable profiles for the large-scale forcings. Yet, with the results of a simulation with these initial profiles, we can further analyze the budget more accurately. In specific, the profiles of the tendencies due to the turbulent heat and moisture flux divergence can be estimated. In addition, better estimates of the tendency due to subsidence can be derived. Still unknown is the tendency profile due to precipitation fluxes, however, considering the small contribution of the precipitation term to the budget, an estimate of 10 Wm^{-2}will be sufficient to use.

In Figure 4.3 the tendencies due to subsidence, advection, radiation and the turbulent fluxes are plotted against height. These tendencies are averages of the last three hours of

the simulation. The net tendencies are also calculated and plotted against height (remind that we ignore the precipitation contribution). These plots evidently show that the cloud and inversion layer are still cooling and moistening, because the temperature and humidity tendencies at a level of about 2 km are still -4 Kd^{-1} and 2-3 $gkg^{-1}d^{-1}$ respectively.

If we vertically integrate these profiles (similar to the integration performed in section 4.1), the budgets for heat and moisture are:

$$-9 \approx -36 + 79 - 69 + 7 + 10 \tag{4.7}$$

$$0 \approx -11 - 129 + 150 - 10 \tag{4.8}$$

Subsidence warming and drying has thus increased, which is due to the stronger temperature and humidity gradients in the inversion layer after the 12 hour simulation. The fluxes are higher as was expected. Yet, the vertically integrated budget for moisture is almost exactly closed, despite the inbalance of the forcings in the cloud layer and inversion. It will be interesting to study the effect of precipitation on these profiles, for example whether it can decrease the strong moistening in the inversion.

Chapter 5

Summary

In this report the preparation of an inititalization set for a new LES intercomparison case is described. The new LES case is an initiative of the GCSS-WGBLC and focuses on the dynamics of precipitating cumuli. It is based on the Rain In Cumulus over the Ocean Experiment, conducted recently in the vicinity of the Caribbean islands Antigua and Barbuda in December 2004 and January 2005. The case is therefore called: the RICO Precipitating Shallow Cumulus Case. Questions that are adressed in this case are related to the ability of different LES model versions to reproduce the mean state of the boundary layer and the amount of precipitation as observed during RICO. Initially it was proposed to base the case on a single day, January 11^{th}, however, for this day the large-scale forcings were difficult to derive and sounding data showed vertical profiles with a weak inversion and high relative humidities. The case is yet based on a three week undisturbed period during RICO (December 16th - January 8th) with typical trade wind cumulus clouds and a modest amount of precipitation (about 0.3 mm/day). Participants of the case are asked to perform a 24 hour LES simulation with the initialization set based on the mean forcings and profiles of this suppressed period.

The initialization set consists of the initial thermodynamic profiles, the large-scale forcings and the desired surface parameters needed to parameterize the surface fluxes. Observations during RICO were used as much as possible to derive these forcings and profiles.

For the initial profiles of potential temperature, specific humidity and the horizontal winds, the dropsondes measurements were used, performed by the NCAR C130 aircraft (on all available flight days (6) within the period of 04/12/16-05/01/08), and radiosondes, launched every 6 or 12 hours from Spanish Point (Barbuda) during that same period. By using the average soundings during the period, initial profiles for LES were constructed.

During RICO, the research vessel Seward Johnson performed measurements from which surface sensible heat and latent heat fluxes are derived. Comparison with the surface fluxes obtained from RACMO showed comparable values. In the proposed simulation the surface fluxes are not fixed but parameterized. Due to the lack of ship measurements in the suppressed period, the sea surface temperature (SST) from the ECMWF analysis is averaged over the three week period.

Unlike the BOMEX case, for which accurate large scale forcings were obtained from an extensive set of observations, reasonable forcings could not yet be deduced from RICO observations. As an alternative, a RACMO HindCast was used to obtain estimates of the

large scale forcings. The RACMO (Regional Atmospheric Climate Model) HindCast is a high-resolution version of the ECMWF model initialized each 24 hours with the ECMWF analysis at 12 UTC. The simulation was performed for a small domain, consisting of 90 x 92 gridpoints with a resolution of 20km, in which the RICO research area (61.46W, 17.97N) is contained. A total period of 2 months (December 2004 and January 2005) was simulated, and output was generated every 10 minutes on a 5 x 5 grid centered around the RICO research area. The output includes, among others, large scale tendencies due to advection (a combined vertical and horizontal advection), vertical profiles of horizontal winds, temperature, moisture and vertical velocity and the precipitation at the surface. A time serie of the latter shows that the relative amount of precipitation produced in RACMO coincides reasonably well with the rainfall observed by the SPolKa radar during RICO, giving a certain confidence in the RACMO results for the undisturbed RICO period. The large scale forcings that are part of the initialization set for LES include the subsidence rate, the large scale temperature tendency due to horizontal advection, the large scale moisture tendency due to horizontal advection and the net radiative temperature tendency.

A budget analysis was performed and RACMO tendencies were used to construct vertical profiles of these large scale forcings. By making a spatial and temporal average, vertical profiles of subsidence and advection were obtained, from which LES profiles were constructed. The subsidence profile shows a downward velocity that is increasing with height, which ensures the (expected) warming and drying in the trade wind layer and is in balance with the radiative cooling. The horizontal advection results on average in a cooling throughout the whole trade wind layer, and a drying in the lower layers and a moistening in the upper layers.

The net radiative tendency was obtained separately by using two offline radiation schemes initialized with the profiles of temperature and humidity from sounding data. By comparing and averaging the results over twenty-four hours, a profile was derived that prescribes a cooling rate of 2 K/day close to the surface, which slightly decreases to about 1 K/day in the free atmosphere.

Combining all these forcings, the budgets for heat and moisture were considered. An additional term for precipitation of 10 W/m2 was included as a sink for moisture and source for heat. This value is based on an average precipitation rate of 0.3 mm/d during the suppressed period obtained from the SPol radar observations. Estimates of tendencies due to turbulent fluxes were derived from LES. The budget analysis led to an almost closed budget for temperature, with radiative cooling and subsidence warming as counteracting forcings in the upper layers, and with advection terms that are in line with the thermal wind estimates. For the moisture budget we reduced the horizontal advective drying in the lowest 1.5 km slightly.

With these adjustments, the forcings balance at almost all levels, except in the inversion layer where a significant cooling and moistening is present of about -4 Kd^{-1} and 2-3 $kgkg^{-1}d^{-1}$. This is also visible in the results of a 12 hour LES simulation, in which temperature and humidity profiles do not change significantly, except in the inversion layer. More specifically, the inversion layer is deepening and getting stronger, and the cloud layer is getting slightly more unstable. This simulation was performed without a microphysics scheme included, and thus no precipitation effects are yet considered.

Appendix A

RICO Operations

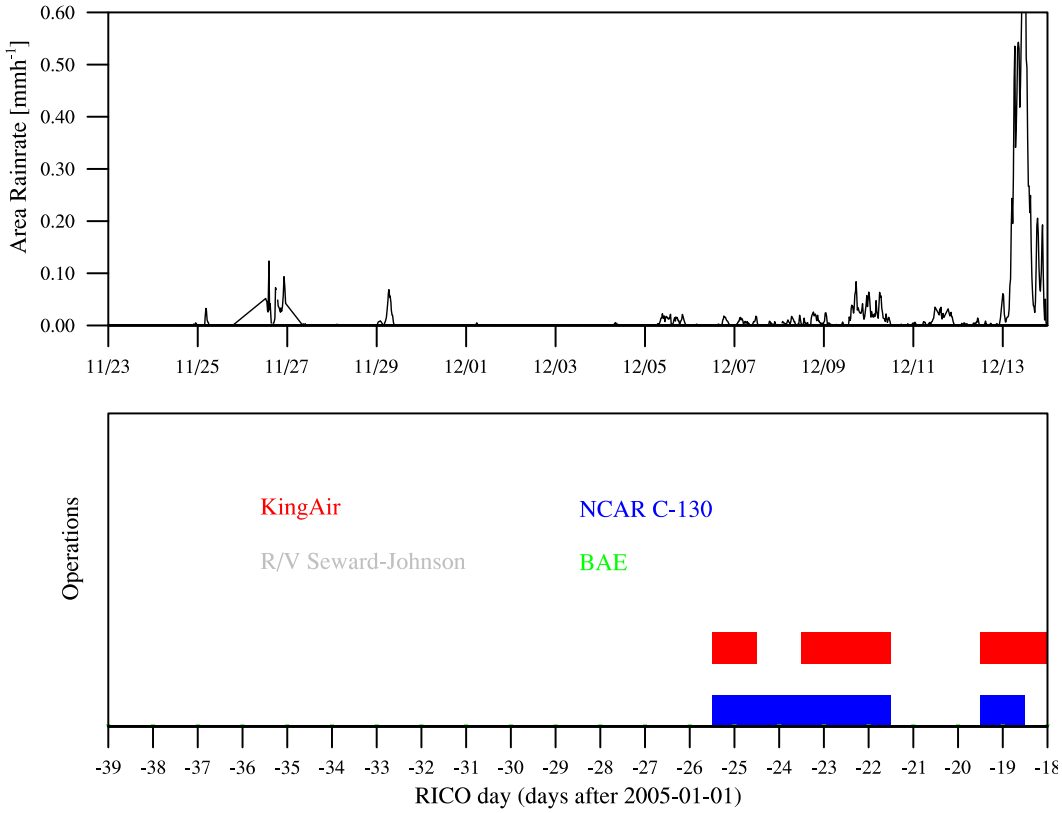

Figure A.1: Area average rainrates in (mmh^{-1}), derived from SPol radar observations for the operational period of the RICO field study (December 2004 - January 2005), are plotted along with the aircraft (NCAR C-130, UK BAE and Wyoming King Air) and ship (R/V Seward Johnson) operations during this same period.

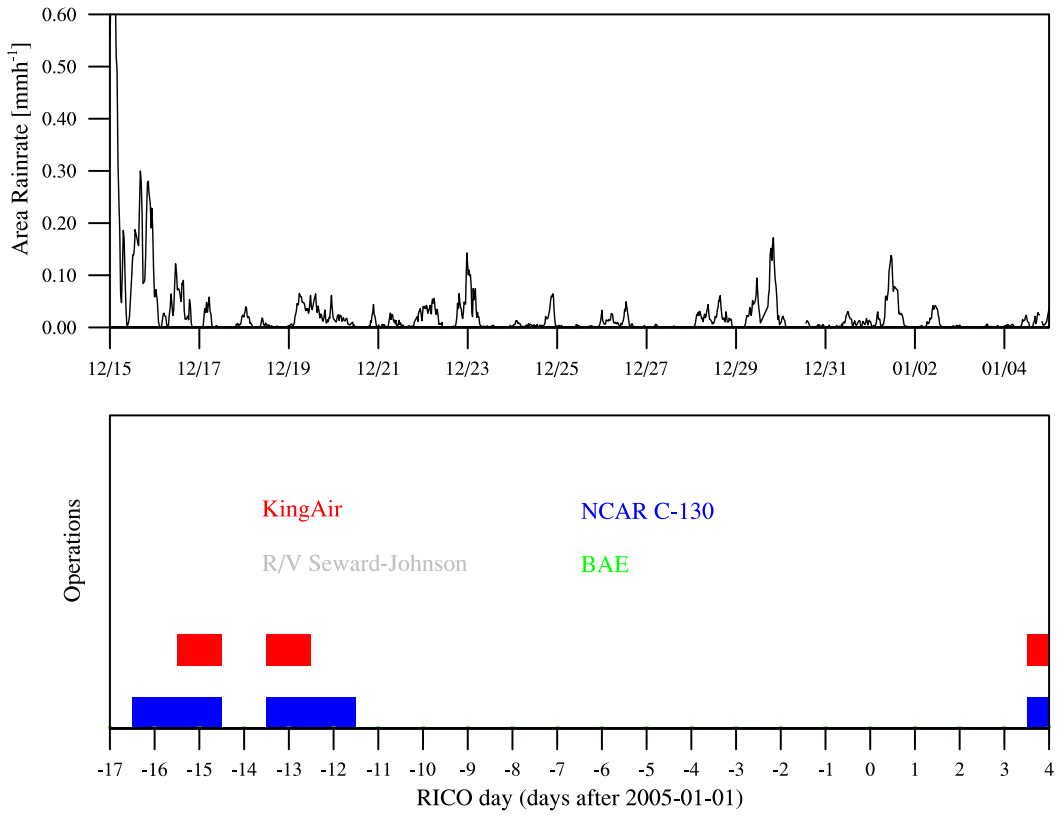
Area Rainrate [mmh-1]
0.60
0.50
0.40
0.30
0.20
0.10
0.00
12/15
12/17
12/19
12/21
12/23
12/25
12/27
12/29
12/31
01/02
01/04
Operations
KingAir
NCAR C-130
R/V Seward-Johnson
BAE
-17 -16 -15 -14 -13 -12 -11 -10 -9 -8 -7 -6 -5 -4 -3 -2 -1 0 1 2 3 4
RICO day (days after 2005-01-01)

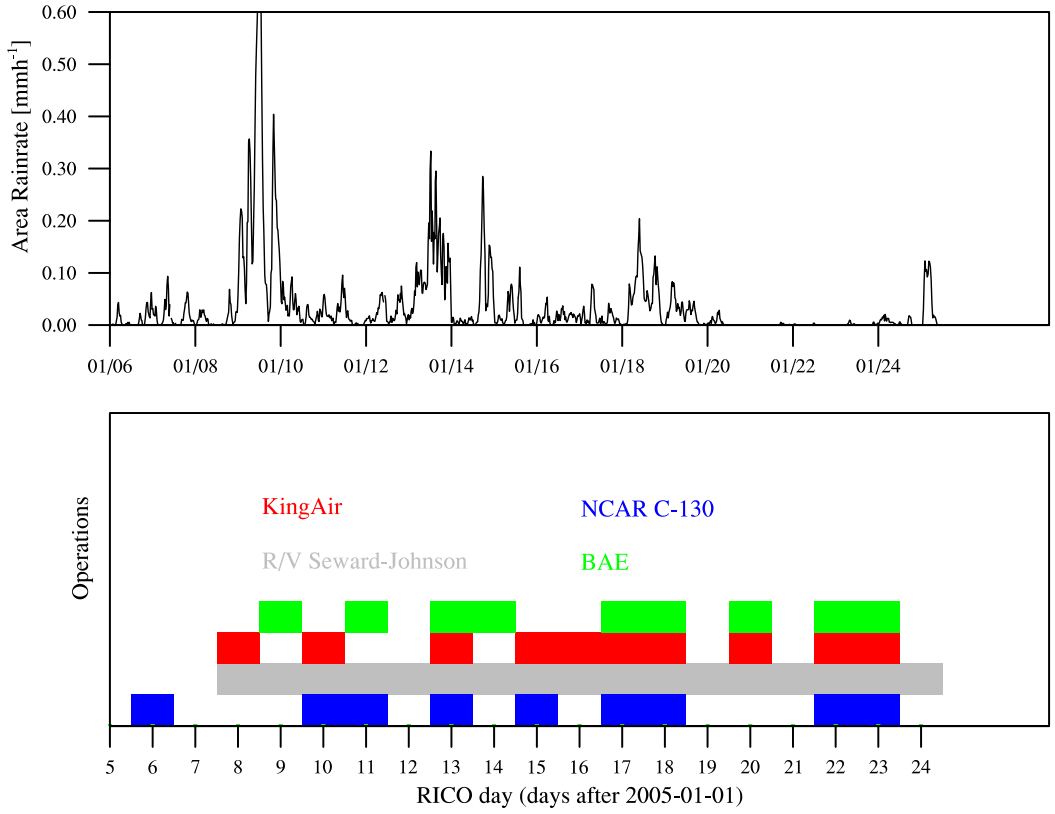
Area Rainrate [mmh-1]
0.60
0.50
0.40
0.30
0.20
0.10
0.00
01/06
01/08
01/10
01/12
01/14
01/16
01/18
01/20
01/22
01/24
Operations
KingAir
NCAR C-130
R/V Seward-Johnson
BAE
5 6 7 8 9 10 11 12 13 14 15 16 17 18 19 20 21 22 23 24
RICO day (days after 2005-01-01)

Appendix B

The derivation of horizontal advection and subsidence from RACMO

The total tendency due to advection is given by the following formula's:

$$\left(\frac{\partial\overline{\theta}_l}{\partial t}\right)_{Total} = -\overline{u}\frac{\partial\overline{\theta}_l}{\partial x} - \overline{v}\frac{\partial\overline{\theta}_l}{\partial y} - \overline{\omega}\frac{\partial\overline{\theta}_l}{\partial p} \tag{B.1}$$

$$\left(\frac{\partial\overline{q}_T}{\partial t}\right)_{Total} = -\overline{u}\frac{\partial\overline{q}_T}{\partial x} - \overline{v}\frac{\partial\overline{q}_T}{\partial y} - \overline{\omega}\frac{\partial\overline{q}_T}{\partial p} \tag{B.2}$$

The two first terms on the right-hand side (rhs) of these equations represent the horizontal advection, the last term on the rhs represents vertical advection *i.e.*, subsidence. The term on the left hand side (lhs) can be obtained directly from RACMO output (by converting temperature tendencies to potential temperature tendencies), but have to be separated into a horizontal and vertical part. The latter, the subsidence, can be estimated from RACMO output as well, by using the vertical velocity omega, ω, in Pas^{-1} and the potential temperature (converted from temperature using the Exner function) and humidity fields. These are available at each of the 40 full levels (in hybrid pressure coordinates) in RACMO. At each level k the subsidence is estimates as:

$$\left(\overline{\omega}\frac{\partial\overline{\theta}}{\partial p}\right)_k \cong \overline{\omega}_k \cdot \frac{\overline{\theta}_{k-1} - \overline{\theta}_{k+1}}{\overline{p}_{k-1} - \overline{p}_{k+1}} \tag{B.3}$$

$$\left(\overline{\omega}\frac{\partial\overline{q}}{\partial p}\right)_k \cong \overline{\omega}_k \cdot \frac{\overline{q}_{k-1} - \overline{q}_{k+1}}{\overline{p}_{k-1} - \overline{p}_{k+1}} \tag{B.4}$$

where q_T is replaced by q for convenience, and it is assumed that $\theta_l \approx \theta$, which is reasonable considering the small liquid water content in cumulus clouds. It is assumed that the pressure jump $\Delta p = \overline{p}_{k-1} - \overline{p}_{k+1}$ is equal for each k.

The tendencies solely due to horizontal advection at each level can yet be obtained:

$$\left(\frac{\partial\overline{\theta}}{\partial t}\right)_{Adv} = -\overline{u}\frac{\partial\overline{\theta}}{\partial x} - \overline{v}\frac{\partial\overline{\theta}}{\partial y} = \left(\frac{\partial\overline{\theta}}{\partial t}\right)_{Total} + \overline{\omega}\frac{\partial\overline{\theta}}{\partial p} \tag{B.5}$$

$$\left(\frac{\partial\overline{q}}{\partial t}\right)_{Adv} = -\overline{u}\frac{\partial\overline{q}}{\partial x} - \overline{v}\frac{\partial\overline{q}}{\partial y} = \left(\frac{\partial\overline{q}}{\partial t}\right)_{Total} + \overline{\omega}\frac{\partial\overline{q}}{\partial p} \tag{B.6}$$

Because LES prescribes the subsidence $\overline{w}_s$ instead of the tendency due to subsidence, this velocity is calculated from the vertical velocity $\overline{\omega}$ in Pas^{-1} from RACMO at each level k as follows:

$$w_{s_k} = \frac{dz}{dt} = \frac{\overline{\omega}_k}{\overline{\rho}_k g} \tag{B.7}$$

where g is the gravitational acceleration (9.8 ms^{-2}) and the air density $\overline{\rho}$ is approximated by:

$$\overline{\rho}_k \cong \frac{\overline{p}_k}{R_d \left(\overline{T}_k \left(1 + 0.61\overline{q}_k\right)\right)} \tag{B.8}$$

where R_d is the gas constant for dry air, and p, T and q are the pressure, temperature and specific humidity at each full level from RACMO.

Temperature advection from the thermal wind relationship

The relationship between the horizontal temperature gradient and the vertical gradient of the geostrophic winds $(\Delta u_g/\Delta z, \Delta v_g/\Delta z)$ is called the thermal wind relationship:

$$\frac{\Delta T_v}{\Delta y} \approx \frac{-f_c T_v}{g} \frac{\Delta u_g}{\Delta z} \tag{B.9}$$

$$\frac{\Delta T_v}{\Delta x} \approx \frac{f_c T_v}{g} \frac{\Delta v_g}{\Delta z} \tag{B.10}$$

where the terms on the lhs represent the large scale horizontal temperature gradients, f_c is the Coriolis parameter (4.5 10^{-5}), T_v is the virtual temperature.

Because the temperature advection (*i.e.*, temperature tendency due to horizontal advection) is defined as the product of horizontal wind and the horizontal temperature gradients, see Equation B.5, its value can be estimated by using observations. The initial profiles of the zonal and meridional wind and their geostrophic components are derived from sounding data as is described in Chapter 3. Estimates of $\Delta u_g/\Delta z, \Delta v_g/\Delta z, \overline{u}$ and $\overline{v}$ are specified in Appendix C and can be used in Equation B.5 to estimate a temperature tendency.

Appendix C

The final LES initialization set

Domain Parameters and Boundary Conditions

- Duration of the simulation: 24 hours
- Domain Size: 12.8 * 12.8 * 4.0 km
- Number of Grid Points: nx = ny = 128, nz = 100
- Implying a Resolution: dx = dy = 100 m, dz = 40 m

Wind and Thermodynamic Profiles

The following initial setup for the horizontal wind components (u, v), the liquid potential temperature (θ_l) and the specific total water content (q_t) is proposed. Other profiles such as pressure, absolute temperature, etc, can be deduced assuming hydrostatic equilibrium. Initially, it can be assumed that there is zero liquid water ($q_l = 0.0$), so that $\theta = \theta_l$ and $q_v = q_t$.

u [m/s]

0 < z < 700	-8.5
z > 700	-8.5 + (-2.0 + 8.5) / (4000 - 700) * (z - 700)

v [m/s]

z > 0	-3.8

q_t **[g/kg]**

0 < z < 540	16.0 + (14.6 - 16.0) / (540) * z
540 < z < 3300	14.6 + (2.4 - 14.6) / (3300 - 540)*(z - 540)
z > 3300	2.4 + (1.6 - 2.4)/(4000 - 3300)*(z - 3300)

θ_l **[K]**

0 < z < 540	297.9
540 < z < 1540	297.9 + (301.7 - 297.9)/(1540 - 540) * (z - 540)
1540 < z < 2100	301.7 + (305.6 - 301.7)/(2100 - 1540) *(z - 1540)
z > 2100	305.6 + (317.0 - 305.6)/(4000 - 2100) *(z - 2100)

Surface Conditions

The sensible and latent heat and momentum fluxes are parameterized in the model, by using a prescribed sea surface temperature (SST) and drag coefficients (C_m = 0.001229 C_h = 0.001094, C_q = 0.001133). The SST is an average of the RICO suppressed period of 2004/12/16 - 2005/01/08.

- SST = 299.8 K
- sea surface potential temperature ths = 298.5 K (with a reference pressure of 1000 mb)
- u* = 0.32 m/s
- z_0 = 1.6 10^{-4} m
- C_m = 0.001229
- C_h = 0.001094
- C_q = 0.001133

Large Scale Forcings and Radiation

The large scale advection and subsidence are based on the analysis of the RACMO Hind-Cast for a 2 months period centered on the RICO Domain. The radiation is based on an offline ECMWF radiation scheme. Both forcings are described in more detail in Chapter ?. The large scale forcings should be applied on q_t, θ_l, u and v.

- **Large Scale Subsidence w [m/s]**

0 < z < 2100	- (0.005/2100) * z
z > 2100	- 0.005 + (0.0003/ (4000 - 2100)) * (z - 2100)

- **Radiative Cooling Rate [K/s]**

0 < z < 3300	- 2 / 86400 + ((-1.1 + 2)/ 86400) /3300 * z
3300 < z < 4000	- 1.1 / 86400 + ((-1.3 + 1.1)/ 86400) /(4000 - 3300) * (z - 3300)

- **Large Scale Horizontal θ_l Advection [K/s]**

z > 0 -0.8 / 86400

- **Large Scale Horizontal q_t Advection [(g/kg)/s]**

0 < z < 550	-1.0 / 86400
550 < z < 1500	-1.0 / 86400 + ((0.0 + 1.0)/ 86400) / (1500 - 550) * (z - 550)
z > 1500	0.0 + (0.7/ 86400) / (4000 - 1500) * (z - 1500)

- **Geostrophic wind x-component u_g**

z > 0 -9.9 + 2.0 * 10-3 * z

- **Geostrophic wind y-component v_g**

z > 0 -3.8

Initial pertubations and translation velocity

The 3d model is initialised with random fluctutions of θ_l and q_t given by:

- θ_l: [-0.1 , +0.1] (K)
- q_t: [-2.5*10^{-2}, +2.5*10^{-2}] (g/kg)

Initial profile of subgrid TKE:
- **TKE**

z > 0 1 - z/4000 m^2/s^2

In order to minimize numerical errors associated with advection we propose to translate the model domain with -6 and -4 m/s in the x and y direction, resp.

Other parameters:

- Latitude: 18.0 N Degr.
- Longitude: 61.5 W Degr.
- Surface pressure: 1015.4 mb

Appendix D

The Atmospheric Research Division at KNMI

This internship is carried out at KNMI, which stands for Royal Netherlands Meteorological Institute and is famous in the Netherlands as the main weather center. KNMI is responsible for daily weather forecasts, and by doing so it serves many different organizations and institutes as the government, the air force, marine force and of course the general public. KNMI does not only provide weather forecasts, moreover, it is the main national center for weather, climate and seismology and it conducts research on a great variety of topics.

The topic of my internship is applicable to climate research and thus I carried out my work at the Atmospheric Research Division, which is part of climate research. The general goal of climate research at KNMI is to observe, understand and predict changes in the climate system. It is carried out as part of international research effort in this field and tries to answer questions regarding global (and local) climate change, the cause of this change and future climate. This is done by acquiring and analyzing observational data through (international) field studies and the set-up of extensive measurement platforms (Cabauw) and by developing regional models to predict natural and anthropogenic variations in the climate in West-Europe.

The Atmospheric Research Division (AO) performs studies on atmospheric energy and water budgets on a local, regional and global scale. Its research is focused on the transport of heat, water vapor and momentum by turbulence and clouds and on the earth radiation budget in relation to clouds, aerosols and greenhouse gases. There is a special focus on the hydrological and energy cycle in the climate system and on fast transport processes that do play a key role in these cycles. More specific, these processes include turbulent and convective transport, clouds and radiation, and land-atmosphere interactions. These are all processes that play a key role in determining climate sensitivity to natural and anthropogenic changes. AO uses its expertise to contribute to the development and evaluation of the atmospheric and soil component in climate models and the application of these models for the use of climate scenarios and climate predictions.

Recently KNMI presented the climate scenarios for the Netherlands for the next 30 years, based on the latest report of the Intergovernmental Panel on Climate Change (IPCC). This panel produces global climate scenarios, which are often not detailed enough to predict the regional climate in the Netherlands. Therefore KNMI uses its own regional models, among which the Regional Atmospheric Climate Model (RACMO), to calculate the scenarios for a smaller region as the Netherlands.

To improve parameterizations of for example turbulence, convection and cloud development in regional models (RACMO), other more detailed models or simulation tools are

used. Large Eddy Simulation (LES) is one of the tools to understand the behaviour of convection on smaller scales (a few hundred meters), which consequently leads to parameterizations of that behaviour on a larger scale in for example RACMO. This also points out the relevance of my study by using observational data (RICO) to set-up a LES simulation for shallow convection and precipitation. Currently, shallow precipitation is not well understood by the research community and improved parameterizations of these processes in RACMO (and other models) are desired. Moreover, the study at AO is performed as part of an international initiative: the GCSS (Global Water and Energy Experiment Cloud System Studies) Working Group on Boundary Layer Clouds, which aims at improving parameterizations in global models (GCM's).

The AO group therefore is an important a link between fundamental research, *i.e.*, the understanding of atmospheric processes, on one side and applied research, *i.e.*, the development of climate models and calculation climate scenarios, on the other side.

Bibliography

Cuijpers, J. and P. Duynkerke, 1993: Large eddy simulation of trade wind cumulus clouds. *J.Atmos.Sci.*, **50**, 3894–3908.

Holland, J. and E. Rasmusson, 1973: Measurements of the atmospheric mass, energy, and momentum budgets over a 500-km square of tropical ocean. *Mon.Wea.Rev.*, **101**, 44–55.

Jensen, J., S. Lee, P. Krummel, J. Katzfey and D. Gogoasa, 2000: Precipitation in marine cumulus and stratocumulus. part I: Thermodynamic and dynamic observations of closed cell circulations and cumulus bands. *Atmospheric Research*, **54**, 117–155.

Lau, K. and H. Wu, 2003: Warm rain processes over tropical oceans and climate implications. *Geophys.Res.Lett.*, **30**(24).

Lenschow, D., P. Krummel and A. Siems, 1999: Measuring entrainment, divergence, and vorticity on the mesoscale from aircraft. *J.Atmos.Oceanic.Technol.*, **16**, 1384–1400.

Petty, G., 1999: Prevalence of precipitation from warm-topped cumulus clouds over eastern Asia and the western Pacific. *J.Climate*, **12**, 220–229.

Short, D. and K. Nakamura, 2000: TRMM radar observations of shallow precipitation over the tropical oceans. *J.Climate*, **13**, 4107–4124.

Siebesma, A. and J. Cuijpers, 1995: Evaluation of parametric assumption for shallow cumulus convection. *J.Atmos.Sci.*, **52**, 650–666.

Siebesma, A. et al., 2003: A large eddy simulation intercomparison study of shallow cumulus convection. *J.Atmos.Sci.*, **60**, 1201–1219.

Stevens, B. et al., 2001: Simulations of trade wind cumuli under a strong inversion. *J.Atmos.Sci.*, **58**, 1870–1891.

Van Zanten, M., 2000: *Entrainment processes in stratocumulus*. Ph.D. thesis, Universiteit Utrecht.

von Salzen, K., N. McFarlane and M. Lazare, 2005: The role of shallow convection in the water and energy cycles of the atmosphere. *Clim.Dyn.*, **25**, 671–688.